Biomaterial multiscale geometry for regenerative immunoengineering of bone tissue

Mooij, Indra; Apachitei, Iulian; Zadpoor, Amir A.; Fratila-Apachitei, Lidy E.

DOI
10.1016/j.actbio.2025.07.036

Publication date
2025

Document Version
Final published version

Published in
Acta Biomaterialia

Acta Biomaterialia 203 (2025) 21–37

Contents lists available at ScienceDirect

Acta Biomaterialia

journal homepage: www.elsevier.com/locate/actbio

Review article

Biomaterial multiscale geometry for regenerative immunoengineering of bone tissue

Indra Mooij [*], Iulian Apachitei, Amir A. Zadpoor [1], Lidy E. Fratila-Apachitei [*,1]

Department of Biomechanical Engineering, Faculty of Mechanical Engineering, Delft University of Technology, Mekelweg 2, 2628 CD Delft, The Netherlands

ARTICLE INFO

Keywords:
Osteoimmunomodulation
surface geometry
coculture
bone regeneration
immunoengineering

ABSTRACT

Osteoimmunomodulation (OIM) is emerging as a key biofunctionality of orthopedic implants. Biomaterial surface geometries can modulate the interactions between immune cells and osteoprogenitors at the bone-implant interface, positively affecting osteogenic differentiation and implant osseointegration. This review highlights the recent advancements in geometry-induced OIM (G-OIM) across multiple length scales (nano to mesoscale, including multiscale topographies and 3D scaffolds), identifying relations between specific geometries and subsequent mechanisms of OIM, as provided by the coculture model used. Our review reveals surface geometries with OIM potential at each length scale. These effects can be mediated by both M1 and M2 macrophages, wherein the pathway depends on the shape and length scale of the geometrical cues provided (*e.g.,* integrin-mediated mechanotransduction for nanoscale topographies and macrophage contact inhibition for micropatterns). Most studies assess G-OIM predominantly based on geometry-induced macrophage polarization and its paracrine effect on osteoprogenitors. However, few studies utilizing direct coculture reveal the key role of the direct interplay between macrophages, osteoprogenitors, and biomaterial for OIM. The novel field of G-OIM is advancing at a high pace. It could benefit from improved, clinically relevant coculture models involving human-derived cells and technological developments in biomaterial design and fabrication. Such advances could establish (G-)OIM as a transformative approach for regenerative immunoengineering of orthopedic implants.

Statement of significance: Osteoimmunomodulation, the ability of biomaterials to modulate the interactions between immune cells and skeletal cells to enhance osteogenesis, is increasingly recognized as a crucial biofunctionality for orthopedic biomaterials. Various biomaterial surface geometries can be used to target osteoimmune pathways. Given the complexity of these interactions, suitable coculture models are essential for studying the underlying cellular mechanisms. This review reveals the state-of-the-art results on geometry-induced osteoimmunomodulation. Not only does this review discuss approaches that have been taken thus far in terms of biomaterial geometry design at various length scales, but it also highlights the role of the coculture model in osteoimmunomodulation and the importance of advances in these *in vitro* models to improve the translation of research to clinical practice.

List of abbreviations: ALP, Alkaline Phosphatase; ARS, Alizarin Red staining; BCP, Biphasic Calcium Phosphate; BMP-2, Bone Morphogenetic Protein 2; Bsp, Bone sialoprotein; COL1, Type I collagen; Dlx5, Distal-less homeobox 5; ECM, Extracellular Matrix; eNOS, Endothelial nitric oxide synthase; G-OIM, Geometry-induced osteoimmunomodulation; HA, Hydroxyapatite; HUVEC, Human Umbilical Vein Endothelial Cell; IAI, Implant-associated infections; iNOS, Inducible Nitric Oxide Synthase; MAO, Micro-arc oxidation; MAPK, Mitogen-Activated Protein Kinase; MCM, Macrophage-conditioned medium; MSC, Mesenchymal Stromal Cell; NF-κB, Nuclear factor kappa-light-chain-enhancer of activated B cells; MyD88, Myeloid differentiation primary response 88; NFATc1, Nuclear factor of activated T-cells c1; NO, Nitric oxide; OCN, Osteocalcin; OIM, Osteoimmunomodulation; ON, Osteonectin; OPN, Osteopontin; OSM, Oncostatin M; OSX, Osterix; PCL, Polycaprolactone; PEEK, Polyetheretherketone; PI3K, Phosphoinositide 3-Kinase; PKA, Protein Kinase A; RhoA/ROCK, Ras Homolog Family Member A/Rho-Associated Protein Kinase; RUNX2, Runt-Related Transcription Factor 2; TGF-β, Transforming Growth Factor-Beta; Ti, Titanium; TLR, Toll-Like Receptor; TNF-α, Tumor Necrosis Factor-alpha; TNTs, Titanium nanotubes; VEGF, Vascular Endothelial Growth Factor.

* Corresponding authors.
E-mail addresses: I.Mooij@tudelft.nl (I. Mooij), E.L.Fratila-Apachitei@tudelft.nl (L.E. Fratila-Apachitei).
[1] Joint last authors.

https://doi.org/10.1016/j.actbio.2025.07.036
Received 11 March 2025; Received in revised form 26 June 2025; Accepted 15 July 2025
Available online 16 July 2025

1. Introduction

Bone defects affect millions of people worldwide [1]. Natural bone grafts are the primary course of action for small-size defects [2,3]. However, auto/allo/xenografts are insufficient for regeneration of critical-size bone defects, due to limited graft availability, donor site morbidity and the risk of immune rejection in the case of allografts and xenografts [2,3]. Therefore, implants made of suitable biomaterials are necessary. Over the years, orthopedic biomaterials have transitioned from bioinert to osteoconductive and osteoinductive [4]. Strategies, such as using bone-resembling ceramics or designing bone ingrowth-allowing structures, have enhanced osseointegration [3,5–8]. Still, the translation to the clinical setting is slow [9]. Lack of understanding of the biological processes at the bone-implant interface and insufficiently relevant *in vitro* and *in vivo* models are among the bottlenecks hindering translational research [10].

Developments in bone biology have shown that osteogenesis is more intricate than previously thought, as it is heavily interwoven with the immune system [9–12]. Osteoimmunology (*i.e.,* the study of bone metabolism regulation by the immune system), coined in 2000 by Takayanagi *et al.* [13], is evidenced by various osteoimmune signaling pathways regulated by immune cells [9–12]. In addition to this interplay, in the case of bone implants, the nature of the immune response to the implant is critical for the rate of osseointegration [9]. Prolonged inflammation and the formation of a fibrous capsule prevent the implant from integrating with the surrounding bone, which may ultimately lead to implant loosening [10]. Therefore, understanding the interplay between biomaterials, immune cells, and skeletal cells is essential for achieving osseointegration. This led to the concept of "osteoimmunomodulation" (OIM), introduced in 2016 by Chen *et al.* [9], which describes the ability of a biomaterial to modulate the local immune response to achieve a pro-osteogenic microenvironment. Since then, various strategies have been used to accomplish this biofunctionality, such as (bio)chemical and physical modification of biomaterials, and interfacing these biomaterials to immune cells, predominantly macrophages [9,12]. Depending on their polarization state, macrophages can stimulate inflammation (M1) or tissue repair/remodeling (M2) [14]. Both phenotypes and subcategories secrete specific cytokines, chemokines, and osteoinductive factors, such as bone morphogenetic protein 2 (BMP-2) and oncostatin M (OSM). These factors influence other immune cells, recruit mesenchymal stromal cells (MSCs), and promote their differentiation into osteoblasts [10].

Following the discovery that both osteogenic differentiation of osteoprogenitors and macrophage activation can be guided using biomaterial geometry, various geometrical approaches have been explored for these separate goals, paving the way toward OIM (Fig. 1 [9, 13,15–20]).

Recent advancements in biofabrication enable the development of highly defined geometries for a wide range of biomaterials. Unlike chemical modifications, geometry-induced OIM (G-OIM) does not require extra biomaterials or bioactives [21] and provides a stable interface with relatively fewer side effects locally or systemically, as reported with clinical use of growth factors like BMP-2 [22]. However, recent data obtained from monocultures suggests that macrophages may be responsive to different geometries than MSCs [19,23], posing challenges regarding optimizing biomaterial geometry for both cell types. Moreover, compared to geometry-induced effects in monocultures, G-OIM in cocultures of MSCs and macrophages has been explored to a lesser extent. In fact, in the absence of a biomaterial, it has been established that coculture with macrophages significantly increases the osteogenic differentiation of MSCs and mouse preosteoblasts (MC3T3-E1s) compared to monoculture, with varying osteogenic potential depending on the macrophage polarization state [24,25]. As biomaterial geometry can direct macrophage polarization, the secretion of (anti-)inflammatory and osteogenic cytokines can be regulated. Therefore, an osteogenic peri-implant environment can be created to sustain OIM. Such biomaterials are considered osteoimmunomodulatory, and, in this case, the primary cue through which this biofunctionality is achieved is their geometry.

This paper reviews the recent findings and trends in G-OIM, using coculture studies that used physical cues to provoke OIM. Therefore, the biomaterial geometries were grouped into three different categories, as follows: topographies with nano-, submicron- and microscale surface features; multiscale topographies (*i.e.,* surfaces with a combination of nano- and microscale features); and 3D biomaterial geometry (*i.e.,* porous scaffolds). The induced effects on immune cells and osteoprogenitors, together with the underlying molecular mechanisms revealed by the coculture models, are discussed. Finally, challenges and future perspectives related to both G-OIM and coculture models necessary for advancing the research in the field are addressed.

2. General overview

From the analyzed literature, it is evident that research on G-OIM started in 2017 and has been on a steady increase since (Fig. 2A). Most of the research was focused on nano- and microscale topographies, followed later by multiscale topographies and scaffold geometries (Fig. 2B). The most used biomaterials were titanium (Ti) and its alloys, followed by ceramics (Fig. 2C). The vast majority of the studies evaluated G-OIM using indirect coculture models based on macrophage conditioned medium (MCM) (Fig. 2D). Only 2 studies utilized direct coculture models (*i.e.,* models in which the two types of cells were cocultured on the same sample) [26,27]. Most cells were of murine origin (Fig. 2E). This was especially true for immune cells, with RAW264.7 macrophages being dominant. Only one study used human monocyte (THP-1) derived macrophages [26]. Primary immune cells were only used in two studies, in the form of primary murine macrophages (mBMDM) [28,29]. In terms of skeletal cells, MSCs of different origins were most frequently used, followed by murine preosteoblasts (MC3T3-E1) and human osteosarcoma cells (SaOS-2) (Fig. 2E). The most common coculture combination was murine MSC with murine RAW264.7 (Fig. 2F). Of note, combinations of human and murine-derived cells were reported in six studies (RAW264.7 + SaOS-2 or RAW264.7 + hMSC) [30,31–35].

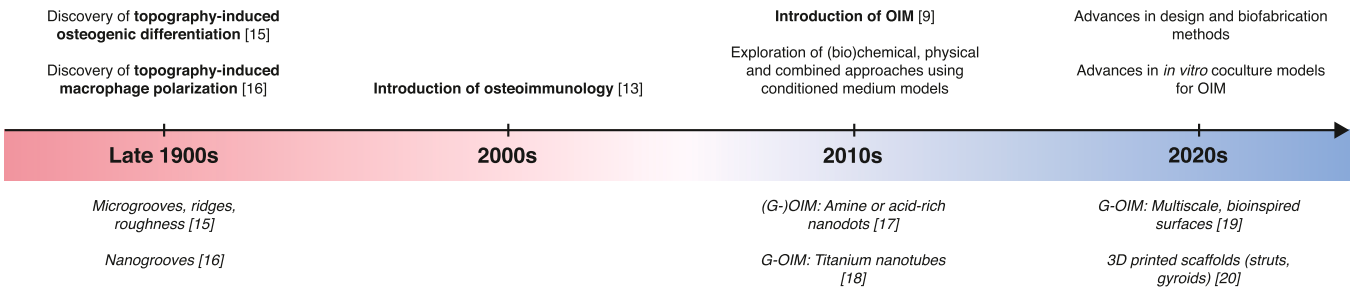

Fig. 1. Timeline of advances in geometry-induced osteogenesis, geometry-induced macrophage polarization, and geometry-induced osteoimmunomodulation (G-OIM).

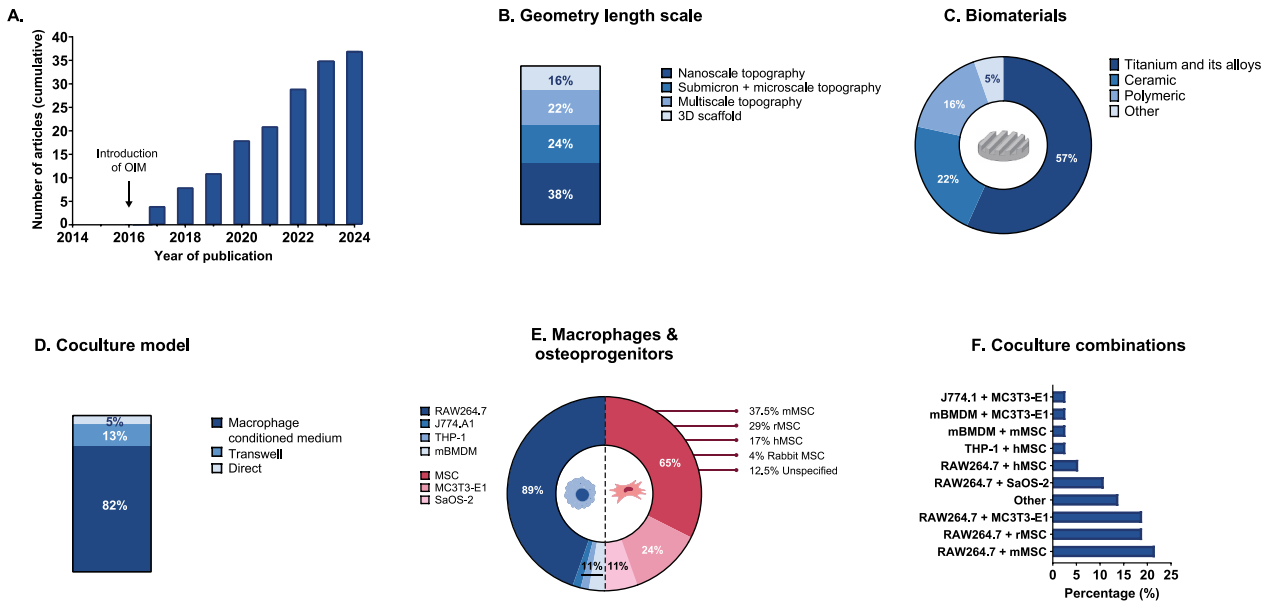

Fig. 2. A general overview of the findings: (A) cumulative number of articles; (B) length scales of the geometries investigated; (C) type of biomaterials studied; (D) type of coculture model used in the studies; (E) immune cells and skeletal cells involved in the studies; (F) the reported combination of cells in the coculture models.

2.1. Surface topographies for G-OIM

2.1.1. Nanoscale topographies

Most of the research regarding G-OIM has been focused on nanoscale topographies (Table 1). As macrophages optimally sense and respond to features in this size range, this approach for immunomodulation was repeatedly observed. The most studied nanoscale topographies were titanium nanotubes (TNT) with diameters between 21 and 200 nm [18,28,36–41]. For OIM, all nanoscale topographies were evaluated using indirect coculture systems, primarily MCM. Two studies used transwell systems to assess MSC migration from the insert in the presence of macrophages cultured on biomaterials in the bottom chamber [39,42]. The OIM nanoscale topographies affected macrophage polarization through mechanotransduction, presumably activated due to the closeness of surface feature sizes to macrophage filopodia (100-300 nm diameter [43]) and cellular receptors [3]. Indeed, M1 and M2 polarization were achieved by regulating specific macrophage integrin subunits. The anti-inflammatory microenvironments promoted osteogenesis of MSCs, MC3T3-E1s, and SaOS-2.

2.1.1.1. Titanium nanotubes. Across three independent studies, TNTs with diameters in the 70–110 nm range consistently induced M2-mediated osteogenesis [37–39], although ⌀ 30 nm TNTs achieved comparable or superior effects depending on the cell source and coculture model (Table 2) [28]. Shen *et al.* [39] observed an early M1 response on ⌀ 110 nm TNTs, driven by integrin upregulation and Nuclear factor kappa-light-chain-enhancer of activated B cells (NF-κB)/Mitogen-Activated Protein Kinase (MAPK) signaling (Fig. 3A). The secreted M1 cyto- and chemokines promoted rMSCs migration in a transwell system. Within 72 hours, coculture presumably triggered an M2 shift, yielding higher alkaline phosphatase (ALP) activity and mineralization than ⌀ 70 nm and ⌀ 30 nm TNTs or flat Ti. Two MCM studies using similar diameters of TNTs ([38,37]) further supported the potential of this diameter range: ⌀ 70 nm TNTs elicited the most pronounced M2 polarization of RAW264.7, leading to the highest osteogenic gene expression in MC3T3-E1 [38] and rMSCs [37], followed by ⌀ 100/110 nm and then ⌀ 30 nm TNTs.

In contrast, Wang *et al.* [28] found that ⌀ 30 nm TNTs outperformed ⌀ 100 nm TNTs in both a MCM model and in a murine calvaria model, despite ⌀ 100 nm TNTs elevating Runt-Related Transcription Factor 2 (Runx2) and Bmp2 in mMSC monoculture and falling in the previously mentioned size range. Primary mBMDMs adopted a dominant M2 phenotype on ⌀ 30 nm TNTs as opposed to M1-polarization on ⌀ 100 nm TNTs, and yielded a higher *in vivo* bone volume fraction. This notable discrepancy could stem from two variables absent in the other studies: the primary macrophage origin and the *in vivo* model. Notably, osteogenesis still proceeded *via* an M2-mediated mechanism, although being triggered by the ⌀ 30 nm TNTs.

Collectively, these data indicate that M2-polarizing TNTs are optimal for G-OIM osteogenesis, while an initial M1 response may be advantageous for recruiting MSCs and amplifying subsequent osteogenesis. TNTs of ⌀ 70–110 nm achieved M2-G-OIM most frequently, while the contrasting ⌀ 30 nm TNTs by Wang *et al.* [28] emphasize the influence of cell source (primary *versus* isolated) and biologically relevant culture conditions.

2.1.1.2. Nanorods and nanowires. Similarly, nanorods and nanowires induced M2-mediated osteogenesis, confirmed *via* BMP-2 and transforming growth factor-beta (TGF-β) osteogenic signaling pathways. In both cases, immunomodulation occurred through integrin-mediated M2 polarization. In a study by Yu *et al.* [42], 85 nm interspaced nanorods of ⌀ 70 nm (Fig. 3B) upregulated RAW264.7 Itga5 and Itgb1 and the phosphatidylinositol 3-kinase (PI3K)/Akt1 pathway in response to increased fibronectin adsorption on the topography. In a transwell coculture, this led to enhanced BMP-2 secretion compared to macrophages on 0 nm interspaced rods. A positive effect of macrophage Itga5 upregulation for G-OIM has also been noted by Li *et al.* [44], comparing nanowires to nanonests and nanoflakes (Fig. 3C). Nanowires downregulated pro-inflammatory cytokine genes, while upregulating Tgfb and promoting the highest osteogenic gene expressions *via* the BMP-2/SMAD pathway in MCM.

Altogether, the studies utilizing nanoscale topographies demonstrate that G-OIM can be achieved through M2 polarization, which was repeatedly induced *via* integrin (Itga5 and Itgb1)-mediated mechanotransduction. In particular, feature sizes in the range of 70-110 nm have been found successful across substrates, potentially due to closeness in size to macrophage adhesion complexes. This theory requires further investigation, in combination with the observation that primary murine macrophages responded vastly different than the RAW264.7 cell line [28], which was used in all other studies [36–41]. Upon M2 polarization

Table 1
Summary of the studies focused on nanoscale topography-induced OIM.

Geometry	Feature size	Biomaterial	Fabrication method	Coculture system	Cells	Polarization result	Osteogenic readouts	Ref
Nanotubes	21, 63, 134 nm diameter	Ti6Al4V, BMP-2 incorporated**	Anodic oxidation	MCM	rMSC, RAW264.7	134 nm: M2-like	134 nm: ↑ Osteogenesis (Alp, Col1a, Bsp, Runx2, ARS)	[36]
	30 & 100 nm diameter	Ti	Acid etching and anodic oxidation	MCM*&***	mMSC, mBMDM	30 nm: M2	30 nm: ↑ Osteogenesis (Bmp2, Runx2, ALP activity, ALP staining)	[28]
	30-40 & 70-80 nm diameter	Ti	Acid etching and anodic oxidation	MCM	MC3T3-E1, RAW264.7, HUVEC	70-80 nm: M2	70-80 nm: ↑ Osteogenesis (Colx, Ocn, Opn, ALP activity, ALP staining) ↑ Angiogenesis (Platelet-derived growth factor, VEGF, tube formation, wound closure)	[18]
	30, 70, 100 nm diameter	Ti, Zn-incorporated**	Anodic oxidation, hydrothermal treatment	MCM*&***	MC3T3-E1, RAW264.7	70 nm: M2	70 nm CM: ↑ Osteogenesis (Alp, Opn, Runx2, ALP activity, ALP staining)	[38]
	~100 nm diameter	Ti, Hydrogenated TNT**	Anodic oxidation	MCM*	MC3T3-E1, RAW264.7	TNTs: M2	TNTs: ↑ Osteogenesis (Bmp2, Ocn, ALP activity, ARS)	[40]
	30, 70, 110 nm diameter	Ti	Anodic oxidation	Transwell	rMSC, RAW264.7	110 nm: M1-M2 shift 24-72h	110 nm: ↑ Osteogenesis (Alp, Col1, Ocn, Opn, ALP activity, ARS) ↑ rMSC migration	[39]
	30, 70, 110 nm diameter	Ti	Anodic oxidation	MCM	rMSC, RAW264.7 HUVEC	70 nm: M2	70 nm: ↑ Osteogenesis (Alp, Bmp2, Ocn, Runx2, COL1, OPN, RUNX2, ALP staining, ARS, Sirius Red S,) ↑ Angiogenesis (BMP2, eNOS, TGFB, VEGF)	[37]
	~100-200 nm diameter	Ti, Mg-incorporated**	Anodic oxidation	MCM	rMSC, RAW264.7	TNTs: M2	TNTs: ↑ Osteogenesis (Alp, Col1, Ocn, Runx2, ALP activity)	[41]
Nanorods	~70 nm rod diameter, 0, 45, 85 nm interrod spacing	Ti	Hydrothermal treatment	Transwell***	MSC, RAW264.7	S85: M1-M2 switch 24-72h	S85: ↑ Osteogenesis (Alp, Opn, Runx2, ALP activity, ARS) ↑ MSC migration	[42]
Nanoparticles (fixed)	16, 38,68 nm diameter nanoparticles Acid-rich or Amine-rich**	Plasma-polymerized allylamine (AApp) or acrylic acid (ACpp) coated, with different sizes gold nanoparticles	Plasma polymerization + nanoparticle immobilization	MCM*	MSC, RAW264.7	All topographies inhibited inflammation compared to flat	68 nm (both chemistries): ↑ Osteogenesis (ARS)	[17]
Nanowires (NW), nanonests (NN), nanoflakes (NF)	NW: 20-40 nm diameter NN: ~500 nm pores NF: 100-200 nm length, ~13 nm thickness, even assembly	Ti	Hydrothermal treatment	MCM*&***	mMSC, RAW264.7	NW: M2	NW: ↑ Osteogenesis (Alp, Col1, Dlx5, Ocn, On, Runx2, ALP activity, ARS)	[44]
Nanostructures	Needle-like (F35, F65), Plate-like (C35, C65)	Calcium deficient HA	Self-setting reaction of a hydraulic α-TCP paste, molding of different pastes (fine or coarse particles)	MCM*	SaOS-2, RAW264.7	No clear link between topography and macrophage polarization	Needle-like: ↑ Osteogenesis (Alp, Bmp2, Bsp, Col1, Ocn, Runx2, ALP staining, ARS)	[33]
Nanopores	0, 50, 100, 200 nm diameter	Al_2O_3	Anodic oxidation	MCM*	rMSC, RAW264.7	100-200: M2 50-100 nm: ↑ Bmp2, Bmp6, Wnt10b	50 nm: ↑ Osteogenesis (COL1, OPN, ARS)	[45]

(*continued on next page*)

Table 1 (*continued*)

Geometry	Feature size	Biomaterial	Fabrication method	Coculture system	Cells	Polarization result	Osteogenic readouts	Ref
Pits (concave) and dots (convex)	60 & 90 nm diameter; 5 & 6 nm depth; 95 & 130 nm interspace (NCPits) 50 & 65 nm diameter; 6 & 9 nm height, 90 & 120 nm interspace (NCDots)	316LSS	Anodic oxidation, immersion-coating	MCM	hMSC, RAW264.7 HUVEC	NCDots: M2	NCDots: ↑ Osteogenesis (OCN, OPN, RUNX2) NCDots: ↑ Angiogenesis (eNOS, Hypoxia-inducible factor 1-alpha, VEGF receptor 2, VEGF)	[31]

* : Osteogenic medium
** : Functionalized version of the same geometry (results not included)
*** : Additional *in vivo* model

Table 2
Main findings of the TNT studies.

Study	⌀ TNT (nm)	Coculture model	Cell types	Polarization outcome	Polarization Mechanism	OIM pathway	Key notes
Shen *et al.* [39]	30, 70, **110**	Transwell	RAW264.7, rMSC	M1 → M2 (72 h)	M1:↑ Itga2, Itga3, Itga5, Itgb2, ↑ NF-κB/MAPK M2 shift: RAW264.7-rMSC interaction	n/a	rMSC recruitment *via* M1 factors (IL-8, stromal cell-derived factor 1 monocyte chemoattractant protein 1) Experiments performed under oxidative stress
Chen *et al.* [38]	30, **70**, 100	MCM*	RAW264.7, MC3T3-E1	M2	-	n/a	Higher protein adsorption on ⌀ 70 TNTs
Tao *et al.* [37]	30, **70**, 110	MCM	RAW264.7, rMSC	M2	↑ Itga5, Itgb3, ↑ FAK-PI3K pathway	n/a	⌀ 70 nm TNTs also induced angiogenesis of HUVECs *In vivo* confirmation
Wang *et al.* [28]	**30**, 100	MCM*	mBMDM, mMSC	M2	-	n/a	Primary macrophage *In vivo* confirmation

* : Osteogenic medium

and the secretion of the osteogenic cytokines BMP-2 and TGF-β, in coculture, osteogenesis was repeatedly enhanced *via* SMAD-dependent pathways in osteoprogenitor cells.

2.1.2. *Submicron and microscale topographies*

The topographies in this section span the subcellular to cellular scale and larger. This results in vastly different mechanisms, as interactions between the cells and the substrates differ depending on feature size. At subcellular scale, macrophages detect the topographies using adhesion complexes, whereas at cellular scale and larger, the topographies can induce extended cell spreading in order to "bridge" the topography, or the topography may form a physical barrier, directing collective cell organization. Therefore, this section has been subdivided according to immunomodulation mechanism, from submicron to microscale. The topographies included rough, porous, extracellular matrix (ECM)-mimicking surfaces and controlled micropatterns (Table 3). More varied substrates were investigated compared to nanoscale, including rigid polymers and photosensitive resins [27,46]. Except for one direct coculture study [27], the studies on these length scales relied on MCM to evaluate G-OIM. Altogether, this resulted in alternative mechanisms of G-OIM compared to nanoscale topographies, including M1-G-OIM [34,35,47], macrophage contact inhibition [48], and nitric oxide (NO) metabolism [46].

2.1.2.1. Submicron topographies – integrin signaling. Similar to nanoscale topographies, submicron whiskers induced macrophage cytoskeletal remodeling (*i.e.*, by inducing the formation of pseudopods), affecting macrophage polarization in two independent studies. Using dense and hollow biphasic calcium phosphate (BCP) whiskers, Wu *et al.* [50] and Wang *et al.* [47] uncovered both M1- and M2-mediated osteogenesis (Table 4). Wu *et al.* [50] showed that hollow whiskers induced M2 polarization through modulation of Itga5, Itgav, Itgb1 and Itgb3, of which the MCM enhanced osteogenic gene expressions in MC3T3-E1 through BMP-2/SMAD (Fig. 4A). Similarly, in the study by Wang *et al.* [47], hollow whiskers also induced M2-RAW264.7. Remarkably, higher rates of osteogenesis were observed using solid whiskers, which induced M1-RAW264.7 with elevated tumor necrosis factor-alpha (TNF-α) secretion and branched pseudopods. This morphological change was suspected to play roles in the determining course of polarization. The inflammatory MCM promoted migration and osteogenic differentiation of MSCs, uncovering TNF-α-mediated osteogenesis, which is not commonly recognized for osteogenic properties. Despite the different mechanisms of G-OIM, the whisker surfaces that promoted the strongest osteogenesis in both studies displayed the highest serum protein adsorption and also performed optimally *in vivo* in both studies.

The study by Zhu *et al.* [49] nicely demonstrated how mechanisms of cell-substrate interactions and immunomodulation alter depending on the length scale of the same topography. This was evaluated using honeycombs spanning from nano- to microscale (Fig. 4B). Briefly, smaller scale honeycombs (⌀ 90 and 500 nm) were OIM by supporting RAW264.7 spreading and filopodia formation, leading to M2 polarization and BMP-2-mediated osteogenic differentiation of mMSCs in MCM. The formation of filopodia on the ⌀ 90 nm honeycombs was attributed to the activation of the Ras homolog family member A/Rho-associated coiled-coil containing protein kinase (RhoA/ROCK) pathway by the topography. Additionally, nanoscale honeycombs upregulated genes related to the regulation of the cytoplasm, cytoskeleton, and podosome, as well as members of the peroxisome proliferator-activated receptor signaling pathway, involved in M2 polarization [52]. Therefore, ⌀ 90–500 nm honeycombs fall within the gripping width of macrophage filopodia, activating mechanotransduction for M2. Above ⌀ 500 nm, the researchers note that the macrophages were less able to spread over the topographies and had significantly reduced filopodia formation, resulting in M1 polarization. This demonstrates a clear differences in cell-substrate interactions above submicron scale.

2.1.2.2. Submicron pores – nitric oxide (NO) metabolism. Whereas many of the above studies relied on BMP-2 or TGF-β-mediated osteogenesis, another M2-G-OIM mechanism was uncovered by Liu *et al.* [46] using submicron porous polyetheretherketone (PEEK) and porous composites

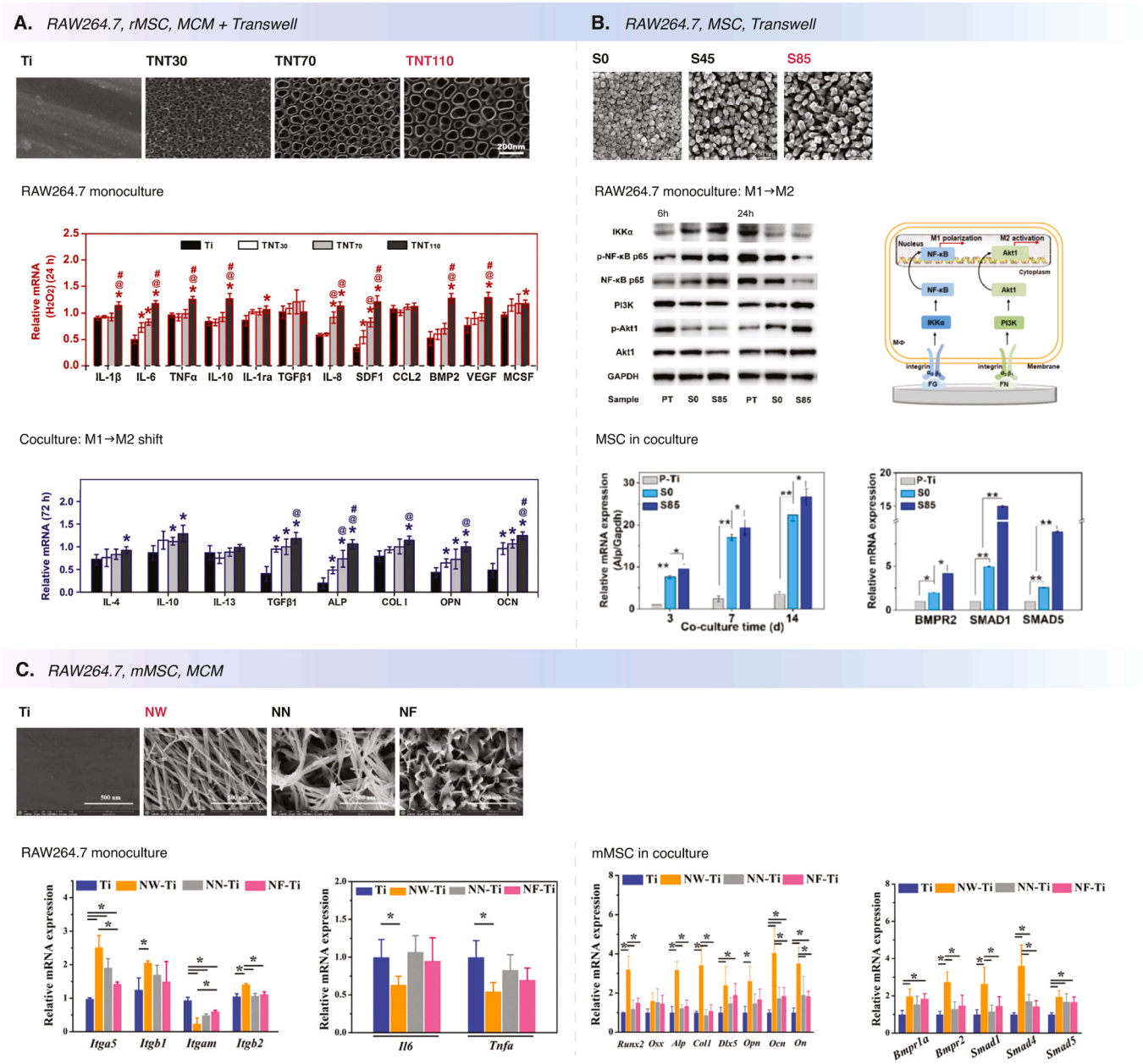

Fig. 3. Highlighted findings and mechanisms on nanoscale topographies. (A) 110 nm nanotubes induced initial M1 polarization *via* integrin-mediated MAPK and NF-κB pathways, leading to enhanced rBMSC migration *via* secreted chemoattractants and immunoregulation. Adapted with permission from [39]; (B) 85 nm interspaced nanorods activated the PI3K/Akt1 pathway in RAW264.7, leading to M2-G-OIM in MCM through BMP-2/SMAD signaling. Adapted with permission from [42]; (C) nanowires modulated RAW264.7 integrin expressions and downregulated inflammatory gene expressions, which MCM promoted osteogenic gene expressions through BMP-2/SMAD signaling in mBMSC. Adapted with permission from [44]. Copyright 2025 American Chemical Society.

of PEEK with hydroxyapatite (HA-PEEK) (Fig. 4C). As HA-PEEK inhibited the NO secretion of RAW264.7 *via* inducible Nitric Oxide Synthase (iNOS), protein kinase A (Pka), Runx2, Osterix (Osx) and Alp were upregulated in mMSCs in response to this MCM with decreased NO. This was caused by the involvement of NO in the cAMP-PKA signaling pathway in mMSCs, affecting Runx2 transcription [53].

2.1.2.3. Microscale patterns – collective macrophage organization. As the study by Zhu *et al.* [49] indicates, at microscale, the interactions between macrophages and the topography vastly differ from nano/-submicron scale. When macrophages can no longer bridge and "grasp" the topography, other mechanisms come into play. In two studies utilizing micropatterns, macrophage organization was guided by the topography, affecting cellular contact. Zhang *et al.* [48] found that Ti grid micropatterns stimulated M2-G-OIM through inhibition of RAW264.7 cell-cell contact (Fig. 4D). Inhibited contact because of the surface geometry caused loss of E-cadherin and translocation of β-catenin from membrane regions. Nuclear β-catenin downregulated inflammatory genes. Additionally, the micropatterns upregulated anti-inflammatory cytokine genes (amongst others, Bmp2 and Tgfb1), providing a favorable MCM for osteogenic differentiation of mMSCs compared to non-patterned Ti. Another study utilizing micropatterns to direct macrophages' spatial organization facilitated an M1-M2 polarization shift on patterns with subcellular convex areas, leading to M2-G-OIM (Fig. 4E) [51]. When the convex area exceeded the cell area, macrophages displayed rounder shapes with filopodia. In contrast, below the cell area, they became elongated and clustered along the direction of the ridge. The latter patterns initially triggered M1

Table 3
Summary of the studies focused on submicron and microscale topography-induced OIM.

Geometry	Feature size	Biomaterial	Fabrication method	Coculture system	Cells	Polarization result	Osteogenic readouts	Ref
Rough surfaces	Mean roughness values: 432, 307, 224 and 148 nm	Ti	Sandblasting	MCM**	SaOS-2, RAW264.7	432: M1	432: ↑ Osteogenesis (ALP activity, ARS)	[34]
Porous surfaces	Not specified (submicron range)	Sulfonated PEEK, HA composited PEEK (P-HA)	Sulfonation, hydrothermal treatment	MCM	mMSC, RAW264.7	S-PHA: M2-like	S-PHA: ↑ Osteogenesis (Alp, Osx, Runx2)	[46]
		Ti	MAO	MCM*	SaOS-2, RAW264.7	MAO: M1	MAO: ↑ Osteogenesis (ARS, Sirius Red S)	[35]
Honeycombs	Diameters from 90-5000 nm	Ti	Film transfer	MCM**	mMSC, RAW264.7	HC-90: M2	HC-90: ↑ Osteogenesis (Alp, Ocn, Runx2, ALP activity, ARS)	[49]
Submicron pillars	300 nm diameter, 500 nm height, 700 nm interspacing	IP-L780	Two-photon-polymerization	Direct*	MC3T3-E1, J774A.1	Pillars: suspected M1-M0 shift	Pillars: ↑ Osteogenesis (RUNX2)	[27]
Solid and hollow whiskers	Solid whiskers: 13 μm length, 506 nm diameter Hollow whiskers: 573 & 314 nm outer-inner diameter	BCP	Hydrothermal treatment	MCM**	MSC, RAW264.7	Solid whiskers: M1	Solid whiskers: ↑ Osteogenesis (Alp, Col1, Ocn, Opn, ALP staining, ARS) ↑ MSC migration	[47]
	Solid whiskers: 7–10 μm whisker length Hollow whiskers: 2–3 μm whisker length, 0.5–2 μm diameter	BCP	Hydrothermal treatment	MCM**	MC3T3-E1, RAW264.7	Hollow whiskers: M2	Hollow whiskers: ↑ Osteogenesis (Alp, Bmp2, Bsp, Col1, Ocn, Runx2, ALP activity) BMP-2/SMAD	[50]
Grid patterns	Side length of the raised square: 1000 μm, groove width: 300 μm	Ti	Grit-blasting, pattern spraying molten Ti on meshes	MCM	mMSC, RAW264.7	Pattern: M2	Pattern: ↑ Osteogenesis (Alp, Col1, Ocn, Opn, Runx2, ALP staining, ARS)	[48]
Chevron patterns	Decrease of the single convex area, roughness, groove width and height: P1>P2>P3>P4	BCP	Cold isostatic template pressing	MCM	MC3T3-E1, RAW264.7	P3, P4: M1-M2 shift	P3, P4: ↑ Osteogenesis (Alp, Col1, Ocn, Runx2, ALP staining, ARS)	[51]

* : Osteogenic medium
** : Additional *in vivo* model

Table 4
Comparison of the hollow and solid submicron BCP whisker studies.

Study	Feature	Coculture model	Cell types	Polarization outcome	Polarization Mechanism	OIM pathway	Key notes
Wu *et al.* [50]	Solid: 7–10 μm length **Hollow**: 2–3 μm length, 0.5–2 μm ⌀	Transwell	RAW264.7, MC3T3-E1	**Hollow**: M2	↓ Itga5, Itgav, Itgb1, Itgb3	BMP-2/SMAD	Increased fibronectin adsorption on hollow whiskers Hollow whiskers could be grasped by macrophage pseudopods *In vivo* confirmation
Wang *et al.* [47]	**Solid**: 13 μm length, 506 nm ⌀ Hollow: 573 & 314 nm outer-inner ⌀	MCM	RAW264.7, MSC	**Solid**: M1 Hollow: M2	M1: Branched pseudopod formation	TNF-α → RUNX2, OSX	Increased protein adsorption on solid whiskers TNF-α was dose dependent: Above a certain threshold, osteogenesis was reduced through NF-κB *In vivo* confirmation

polarization, though, over time, an increase in TGF-β and a decrease in IL-6 were detected in the MCM, indicating a polarization shift. The MCM of these patterns induced the highest degree of osteogenic gene expression and mineralization for MC3T3-E1.

Several (sub)micron topographies showed OIM potential. Depending on the scale, immunomodulation occurred through vastly different mechanisms. This appears to be determined by how macrophages are able to respond the topography, most evidently demonstrated by Zhu *et al.* [49]. Above submicron scale, macrophage behavior was influenced through fundamentally different mechanisms than at nano- or submicron structures. Organized micropatterns can disrupt or guide collective macrophage organization, modulating polarization through altered cell–cell contact or spatial confinement. This shift from individual to collective responses introduced new osteoimmunomodulatory pathways, *e.g.*, inhibition of E-cadherin/β-catenin signaling [48].

2.1.3. *Multiscale topographies*

As bone consists of nano-, micro-, and mesostructures, a rational design approach combines geometries of multiple length scales on the biomaterial surface. Furthermore, since MSCs and macrophages respond differently to various types and scales of geometries, superimposing nano- on microscale geometries could provide favorable features for both cell types [54]. Such surfaces were investigated in eight studies [19,30,32,29,54–57] (Table 5), of which the majority were represented by micropits decorated with ECM-mimicking nanostructures. These surfaces were evaluated using MCM, except for one study that also used a transwell model [54]. With multiscale topographies, the activation of mechanotransduction pathways such as RhoA/ROCK in macrophage polarization were reported again [56]. The OIM multiscale topographies operated through M2 polarization of macrophages. Subsequent osteogenesis occurred *e.g.,* through the aforementioned pathways of BMP-2 and TGF-β/SMAD.

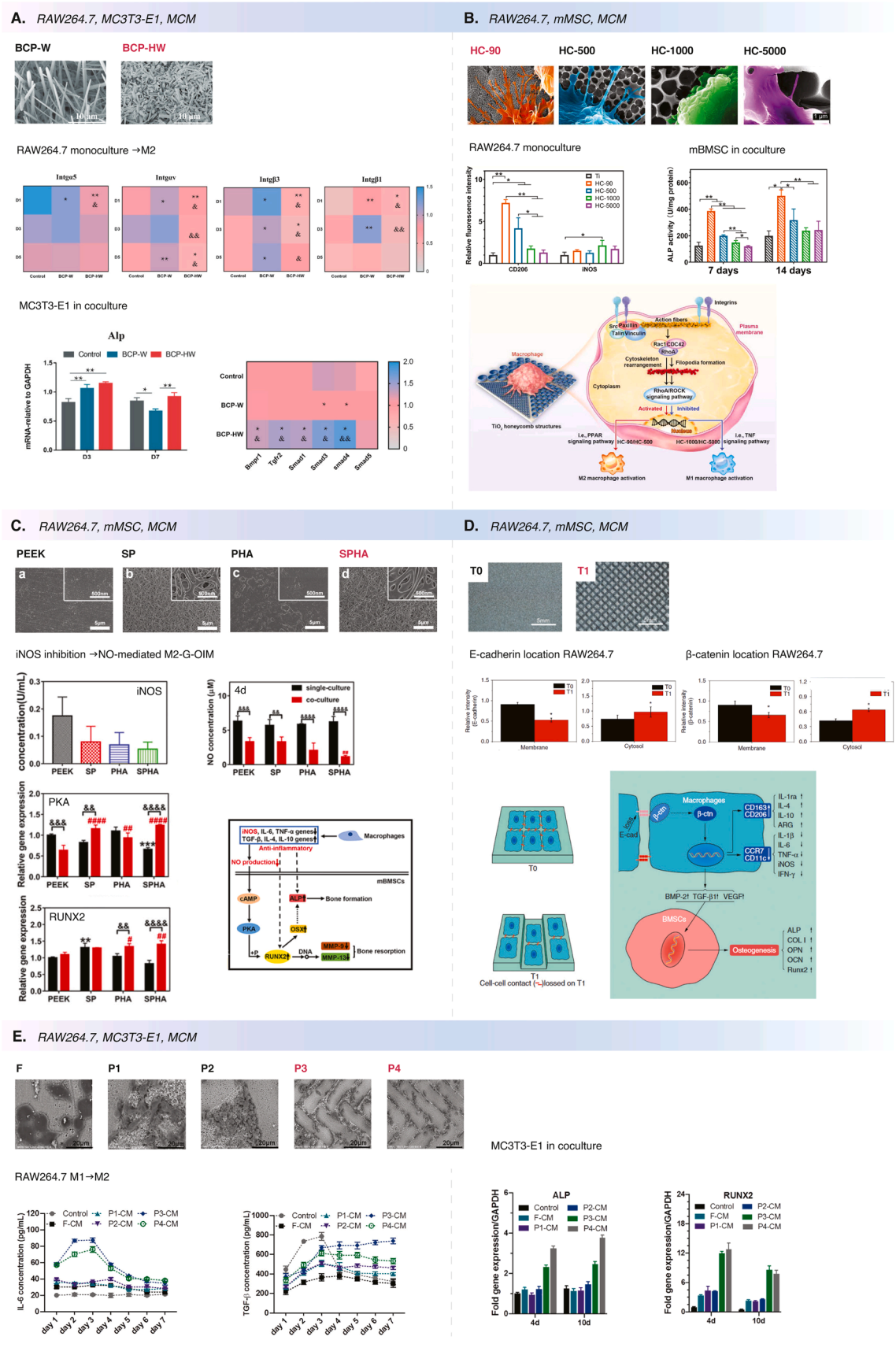

(caption on next page)

Fig. 4. Highlighted findings and mechanisms on submicron and microscale topographies. (A) Submicron whiskers induced M2 polarization by affecting integrins profiles, which resulted in BMP-2 and TGF-β-mediated osteogenesis. Adapted with permission from [50]; (B) different diameters of honeycombs affected macrophage morphology and polarization through regulation of various genes related to the cytoskeleton, resulting in different degrees of ALP activity. Adapted with permission from [49]; (C) submicron pores on HA-PEEK substrates downregulated iNOS and NO secretion of RAW264.7, leading to enhanced RUNX2 expression in mMSCs *via* PKA signaling. Adapted with permission from [46]; (D) macrophage contact inhibition by grid patterns induced M2 polarization through loss of E-cadherin and translocation of β-catenin, leading to enhanced osteogenic gene expression of mMSCs in MCM. Adapted with permission from [48]; (E) Various BCP patterns directed different macrophage organization, which enabled a cytokine shift on P3 and P4, resulting in enhanced osteogenic gene expressions of MC3T3-E1 in MCM. Adapted with permission from [51].

Table 5
Summary of the studies focused on multiscale topography-induced OIM.

Geometry	Feature size	Biomaterial	Fabrication method	Coculture system	Cells	Polarization result	Osteogenic readouts	Ref
Multiscale pits with pores	Not specified	Ti	Electrochemical (CE) followed by acid etching (EE-CE)	MCM***	rMSC, RAW264.7	EE-CE: M2	EE-CE: ↑ Osteogenesis (Col1a, ARS)	[55]
	Primary depressions of 30–50 μm diameter, secondarily depressions of 3–8 μm diameter. Nanopores 50–200 nm diameter.	Ti6Al4V	Sand-blasting, large-grit, acid etching and alkaline thermal treatment	MCM, Transwell	MC3T3-E1, RAW264.7, HUVEC	Multiscale: M2	Multiscale: ↑ Osteogenesis (Bmp2, ARS) ↑ MC3T3-E1 migration	[54]
Microrough substrates with nanopores	Random microroughness with 70 and 90 nm diameter nanopores	Ti	Anodic oxidation	MCM*	MC3T3-E1, mBMDM	TNP-70: M2	TNP-70: ↑ Osteogenesis (Alp, Bmp2, Bsp, Col1, Ocn, Opn, Osx, Runx2, ALP activity, ARS)	[29]
Macroporous surfaces with nanowires	Macroporous Ti (TPS) surfaces with nanowires of 20–50 nm diameter (NTPS)	Ti	Grit-blasting, plasma-spraying	MCM	mMSC, RAW264.7, HUVEC	NTPS: M2	NTPS: ↑ Osteogenesis (Alp, Dlx5, Col1, Oc, On, Opn, Osx, Runx2, ALP staining, ARS) ↑ Angiogenesis (eNOS, p-eNOS)	[56]
Micropits with nanoflakes, nanowires, combination	Nanoflakes (AH0.5) Nanowires (AH5) Nanoflakes and wires (AH3)	Ti	Acid etching and alkali heat treatment	MCM*	SaOS-2, RAW264.7	AH3: M2	AH3: ↑ Osteogenesis (ALP activity, ARS, Sirius Red S)	[32]
Micro@Nanosheets	~75 nm (Nano) & ~0.9 μm (Micro) sheet hexagonal side length ~75 nm & ~0.6 μm sheet hexagonal side length, interspacing ~1.3 μm (M@N)	MgAl sheets on Ti	Hydrothermal treatment	MCM	mMSC, RAW264.7	Nano: M2	Nano: ↑ Osteogenesis (Bmp2, Ocn, Opn, ALP activity)	[57]
Microdots with nanoneedles	5 μm tall nanoneedles on 4, 12, 36 μm diameter microdots of 4 μm height	HA	Photolithography and hydrothermal treatment	MCM	hMSC, RAW264.7 HUVEC	12-Nano, 36-Nano: M2	12-Nano, 36-Nano: ↑ Osteogenesis (BMP2, COL1, RUNX2)↑ Angiogenesis (Basic fibroblast growth factor, eNOS, VEGF)	[30]
Multiscale fibrous patterns	Side length, height, and spacing of the pattern: ~50, 15, 12 μm. Composed of random and aligned fibers: 270 & 30 nm diameter, organized in pattern (P-fiber)	PCL/Gelatin blend, mineralized **	Template-assisted electrospinning	MCM***	rMSC, RAW264.7	P-fiber: M2	P-fiber: ↑ Osteogenesis (ALP activity, ARS)	[19]

* : Osteogenic medium
** : Functionalized version of the same geometry (results not included)
*** : Additional *in vivo* model

Multiscale Ti/Ti6Al4V surfaces that combined acid-etched micropits with nano/submicron pores or nanowires consistently promoted an anti-inflammatory MCM across four studies [32,54–56]. Both Dai *et al.* [55] (Fig. 5A) and Yang *et al.* [54] reported that this M2-MCM enhanced osteogenesis of rMSC and MC3T3-E1 compared to flat, purely micro-, or purely nano-structured controls. In the study by Dai *et al.* [55], the mechanism of immunomodulation was demonstrated to occur through avoidance of Toll-like Receptor 2 (TLR-2) activation, which inhibited pro-inflammatory NF-κB and MAPK pathways. Additionally, the nuclear factor of activated T-cells c1 (NFATc1, master regulator of osteoclastogenesis) was inhibited on the multiscale topography, and no osteoclastic cells were observed. The optimal performance of the multiscale topographies was confirmed in an *in vivo* model. On the multiscale topographies of Pan *et al.* [56], M2-OIM through a BMP-2-dependent pathway was also demonstrated (Fig. 5B). The multiscale surfaces induced elongated and spread macrophages with high intracellular tension, favorable for M2 polarization [32,56]. The involvement of ROCK in M2 polarization was confirmed by using a ROCK inhibitor (Y27632), thereby demonstrating that the addition of nanostructures to micropits enables partly similar macrophage adhesion

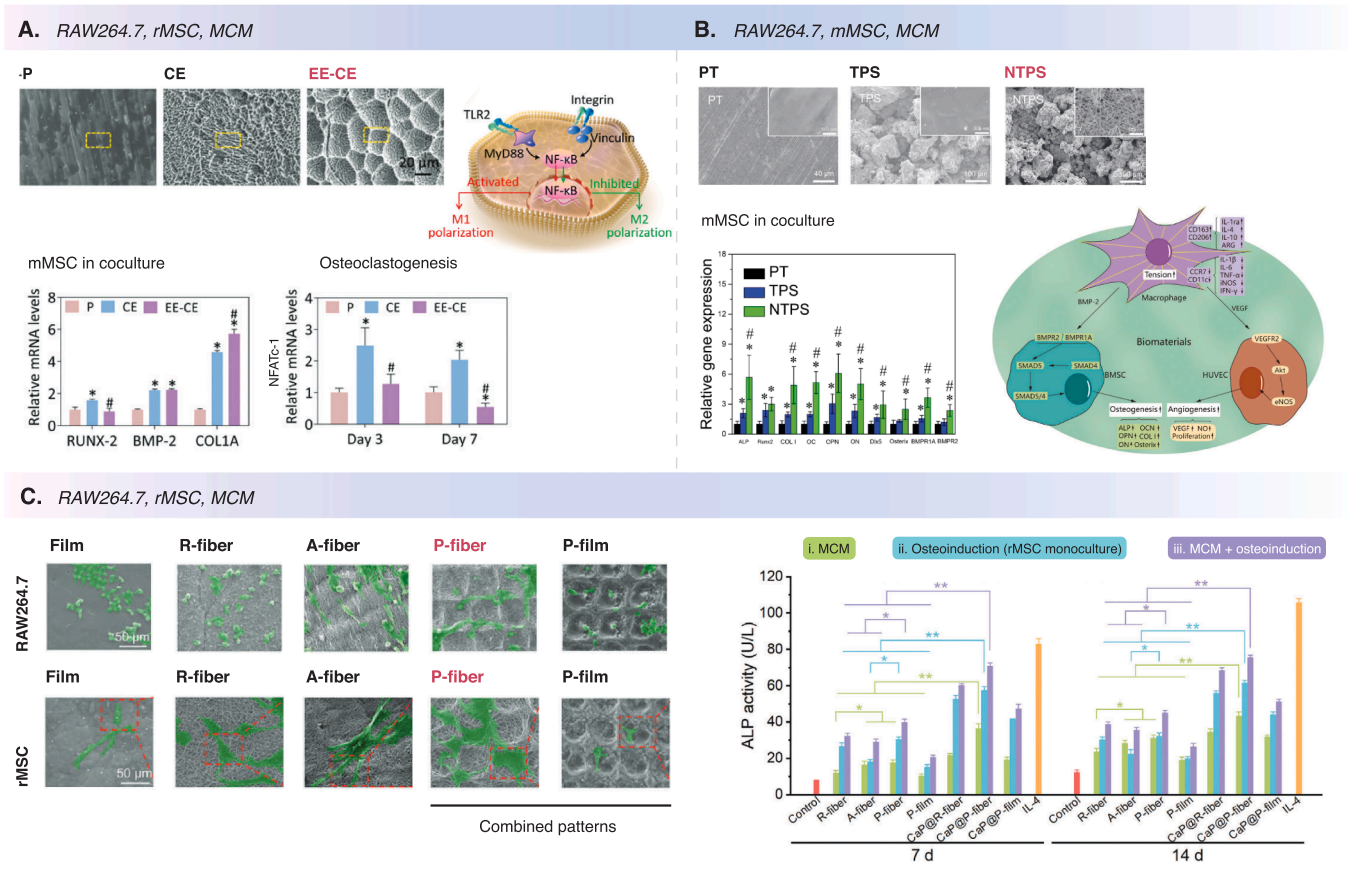

Fig. 5. Highlighted findings and mechanisms on multiscale surfaces. (A) Acid-etched micropits with nanopores inhibited osteoclastogenesis and led to M2 polarization of RAW264.7 by avoiding TLR-2 activation. In MCM, this topography stimulated osteogenesis of rBMSCs. Adapted with permission from [55]; (B) multiscale surfaces with nanowires induced M2 polarization of RAW264.7 *via* increased macrophage intracellular tension, and upregulated osteogenic gene expression of mBMSCs in MCM. Adapted with permission from [56]; (C) multiscale patterns composed of isotropic and anisotropic areas targeted RAW264.7 and rBMSCs differently, and combined patterns led to the highest extent of osteogenesis in an altered MCM model combined for osteoimmunomodulation and osteoinduction. Adapted with permission from [19].

mechanisms as purely nano/submicron topographies.

Exploring the different spatial organization of RAW264.7 and rMSCs on multiscale topographies, He *et al.* [19] found that anisotropic and isotropic areas of electrospun patterns impacted cellular behavior differently for both cell types (Fig. 5C). Anisotropic patterns were favorable for inducing M2-RAW264.7. In contrast, isotropic areas were beneficial for adhesion, spreading, and osteogenic differentiation of rMSCs through contact guidance. Surfaces with mixed patterns of isotropic and anisotropic regions were the most suitable for OIM. All substrates were evaluated at different levels of complexity by using rMSC monoculture, conventional MCM coculture, and an adaptation in which the rMSCs were also cultured on a substrate when receiving MCM (osteoimmunomodulation + osteoinduction, Fig. 5C). The osteogenic potential was the highest in the condition that exposed both cells to the geometry, highlighting the importance of studying the substrate-induced effects on both cell types in parallel with paracrine effects for optimizing OIM.

To conclude, the OIM multiscale topographies provide a favorable environment for M2 polarization of RAW264.7. As with nano/submicron topographies, this involved topography-induced cytoskeletal rearrangement, and occurred through pathways such as RhoA/ROCK, while also suppressing inflammatory and osteoclastic pathways. The microenvironment generated by M2 macrophages enhanced osteogenic differentiation of osteoprogenitors, which repeatedly occurred through BMP-2/SMAD. Importantly, the study by He *et al.* [19] suggests that combined isotropic and anisotropic regions within the same substrate support optimal behaviors in both macrophages and MSCs. This underscores the multifaceted approach that multiscale designs offer.

2.2. Scaffold geometry for G-OIM

Moving one step further toward biomimicry, a fully three-dimensional scaffold with interconnected pores to allow vascularization and bone ingrowth is crucial for the survival of newly created bone tissue and integration with the pre-existing bone. Furthermore, scaffolds should provide the necessary mechanical stability. Beyond mechanical support, these geometries also influence osteoimmune responses. Various pore shapes, sizes, and arrangements have been explored to promote G-OIM, including random *versus* ordered structures and smooth *versus* grooved surfaces [26,58–62] (Table 6). While the exploration of the underlying mechanisms was more limited in the case of scaffolds compared to nano-multiscale topographies, it is evident that scaffold pore morphology can guide macrophage polarization, and that M2 polarization was repeatedly favourable for osteogenesis.

Ordered scaffolds have been realized using a range of biomaterials, including bredigite. The ordered bredigite scaffolds gave rise to a TNF-α low, IL-10 high MCM, which induced osteogenic differentiation of mMSCs [58]. Bmp2 and Runx2 expression and matrix mineralization were elevated compared to random bredigite and dense β-tricalcium phosphate control scaffolds. This was further confirmed *in vivo*. Li *et al.* [60] assessed smooth and grooved pores (Fig. 6A). The grooved scaffold MCM, characterized by lower IL-6, promoted osteogenesis of mMSCs. The underlying mechanism involved the downregulation of miR-214 in mMSCs, which inhibited osteogenesis by suppressing p38/c-Jun

Table 6
Summary of the studies focused on 3D scaffold-induced OIM.

Geometry	Feature size	Biomaterial	Fabrication method	Coculture system	Cells	Polarization result	Osteogenic outcomes	Ref
Scaffolds with particles	Spherical particles (5 & 30 nm diameter), needle-like particles (5 nm diameter)	Collagen scaffold with HA particles	Dehydrothermal treatment, crosslinking	Direct*	hMSC, THP-1	N5: Hybrid phenotypes	Osteogenesis increased significantly for all groups in coculture	[26]
Scaffolds with microgrooves	25–30 μm groove structures	HA	Chitin polymer sol-gel system with W/O emulsion	MCM*	mMSC, RAW264.7	Grooves: Suppress M1	Grooves: ↑ Osteogenesis (COL1, OCN, RUNX2, ALP staining, ARS)	[60]
Gear-shaped grooved scaffold	20 μm grooves	β-tricalcium phosphate	3D printing	Transwell**	Rabbit MSC, RAW264.7	G20: M2	G20: ↑ Osteogenesis (Bmp2, Ocn, Opn, Runx2)	[62]
Scaffolds with controlled pore distribution	400–500 μm pore size (BRT-O), random configuration (BRT-R)	Bredigite	3D printing	CM, Transwell*&**	mMSC, RAW264.7	BRT-O: M2	BRT-O: ↑ Osteogenesis (Bmp2, Runx2, ALP activity, ARS) ↑ mMSC migration	[58]
Scaffolds with controlled pore shapes	500 μm pore size, hexagonal pores (HS) triangular pores (TS)	Ti6Al4V	Selective laser melting	MCM*	MC3T3-E1, RAW264.7	HS: M2	HS: ↑ Osteogenesis (Alp, ALP activity, ARS, Sirius Red S)	[61]
Scaffolds with controlled pore sizes	100, 300, 500 μm pore size	PCL	3D printing	MCM*	MSC, RAW264.7	500: M2	500: ↑ Osteogenesis (ALP activity, ARS)	[59]

* : Osteogenic medium
** : Additional *in vivo* model

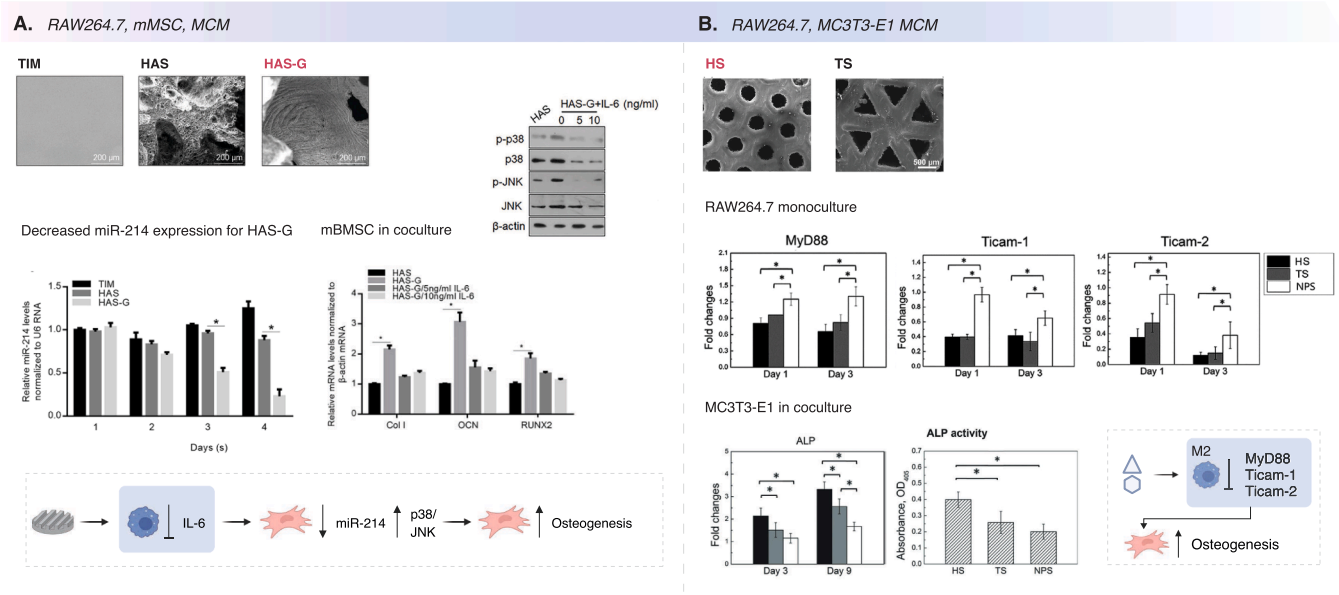

Fig. 6. Highlighted findings and mechanisms on scaffold geometry. (A) Grooved porous scaffolds increased osteogenic gene expression of mBMSCs by reducing the IL-6 levels expressed by macrophages and consequently suppressing miR-214. Adapted with permission from [60]; (B) higher circularity pores were beneficial for inducing M2-mediated osteogenic differentiation of MC3T3-E1s in MCM. Adapted with permission from [61].

N-terminal Kinase [63]. IL-6 is thought to play a role in the upregulation of miR-214; hence, the porous scaffold MCM was favorable.

Regarding pore shape, from a study on hexagonal porous, triangular porous, and dense control Ti6Al4V scaffolds (NPS, Fig. 6B), it was evident that pores with higher circularity induce osteogenesis through M2 polarization of RAW264.7 *via* a TLR-dependent pathway [61]. Both the hexagonal and triangular pores suppressed inflammation compared to non-porous samples, but the effect was stronger for the hexagonal pores. Wang *et al.* [59] developed rectangular pores using polycaprolactone (PCL) scaffolds. Pore diameters from 100 to 500 μm were explored, wherein ⌀ 500 μm pores induced the most matrix mineralization by MSCs in the presence of RAW264.7 CM. In addition, ⌀ 500 μm porous scaffolds induced M2 polarization, markedly reduced TNF-α, and increased IL-10 secretion compared to the other pore sizes. Notably, this is the same pore size as in the bredigite study by Xuan *et al.* [58] and the hexagonal and triangular Ti6Al4V scaffolds [61].

Sridharan *et al.* [26] developed interconnected, randomly organized porous collagen scaffolds decorated with different shapes and sizes of hydroxyapatite (HA) microparticles (spherical and needle-like). In hMSC monoculture, it was evident that the addition of HA increased the osteogenic potential compared to empty collagen scaffolds, most strongly for ⌀ 30 μm spherical particles. Interestingly, when comparing hMSCs monoculture to direct coculture with THP-1 macrophages, calcium deposition increased significantly (up to 2.6 fold), even for scaffolds without HA. This suggests that the induced cellular interactions facilitated by direct coculture were more determinant for osteogenesis than the altered scaffold geometry and composition as a result of the HA particles. Differences in performance between shapes of particles were

not as evident as in hMSC monoculture.

Several trends emerged regarding 3D scaffold geometries. Ordered, interconnected pores of high circularity and diameters around 500 μm were promising for activating M2-G-OIM across various biomaterial substrates. Surface features like grooves further enhanced these effects, *i.e.*, through suppression of pro-inflammatory cytokine IL-6 [61]. Remarkably, direct coculture models, as used by Sridharan *et al.* [26], demonstrate that direct cell communication can outweigh geometrical and biomaterial cues in driving OIM. Future studies should aim to uncover the underlying immunomodulatory and G-OIM pathways, as they were not extensively explored in the studies on scaffolds.

3. Discussion

Modulating the immune response for the recruitment and osteogenic differentiation of osteoprogenitors using biomaterial geometry is a promising approach for the next generation of orthopedic implants. Nevertheless, it involves a complex interplay between biomaterial, immune cells, and skeletal cells, and requires suitable *in vitro* coculture models for investigation. Although the OIM field started less than ten years ago, the results already reveal the strong OIM potential of biomaterial geometry at multiple length scales (Fig. 7). Nano/micro-topographies, multiscale topographies, and 3D scaffold architectures with OIM properties have been evidenced. Nevertheless, the findings so far call for further research using improved coculture models, methodologies, and novel biomaterials to achieve the OIM biofunctionality and understand the underlying mechanisms. *In vitro* models can be further enriched to address unmet clinical needs by integrating antibacterial and angiogenic biofunctionalities alongside OIM properties. Such an approach paves the way toward a novel concept in biomaterial engineering capable of integrating these biofunctionalities. Such biomaterials would enable the precise orchestration of biological events, mirroring the sequence that occurs *in vivo* during tissue regeneration.

3.1. Characteristics of the OIM geometries

Although no conclusive statements can be made regarding the optimal geometry for G-OIM, some characteristics were repeatedly found to be favorable in independent studies, over different substrate compositions and using different cell sources. At the nano to submicron-scale, various topographies with feature sizes within macrophage adhesion complexes (*e.g.*, pseudopods, filopodia, integrins) on different substrates reveal a strong OIM potential (Fig. 7). Successful G-OIM topographies utilizing this mechanism at these scales include *e.g.*, TNTs with diameters between 70 and 110 nm [28,37–40], 85 nm interspaced nanorods of ⌀ 70 nm (*versus* 0 and 45 nm interspace) [42], ⌀ 68 nm nanoparticles (*versus* ⌀ 16 and 38 nm) [17], and honeycombs of ⌀ 90 nm (*versus* honeycombs of ⌀ 500, 1000, and 5000 nm) [49]. Within this scale, geometries displaying similarities to the ECM, such as rods, flakes, sheets, and whiskers, also exhibit potential for OIM. These topographies generally were OIM through an anti-inflammatory environment, except for two transwell models that revealed an M1-M2 shift during coculture [39,42]. As the study by Zhu *et al.* [49] demonstrates, above ⌀ 500 nm, macrophages were no longer able to form filopodia to grasp the honeycomb structure, thereby indicating that above this scale, macrophages interact differently with the geometry. Multiscale topographies consisting of micropits with superimposed nanostructures (*e.g.,* nanopores [54] and nanowires [32,56]) also display OIM, using a similar capacity to influence macrophage behavior for M2 polarization. Therefore, the presence of subcellular structures may provide beneficial geometrical cues for M2-G-OIM in MCM coculture. Furthermore, combining anisotropic and isotropic areas within multiscale topographies has been demonstrated to promote macrophage immunomodulation and osteogenic differentiation of osteoprogenitors, as observed by He *et al.* [19].

Regarding scaffold geometries, the results are more conclusive for determining the characteristics of OIM geometries. Ordered and interconnected porous scaffolds seem more potent than randomly organized scaffolds [58], and pore sizes of ~500 μm were successful in M2-G-OIM in multiple studies [58,59,61]. As a pore size range of 300-600 μm has been previously identified to provide the appropriate balance between

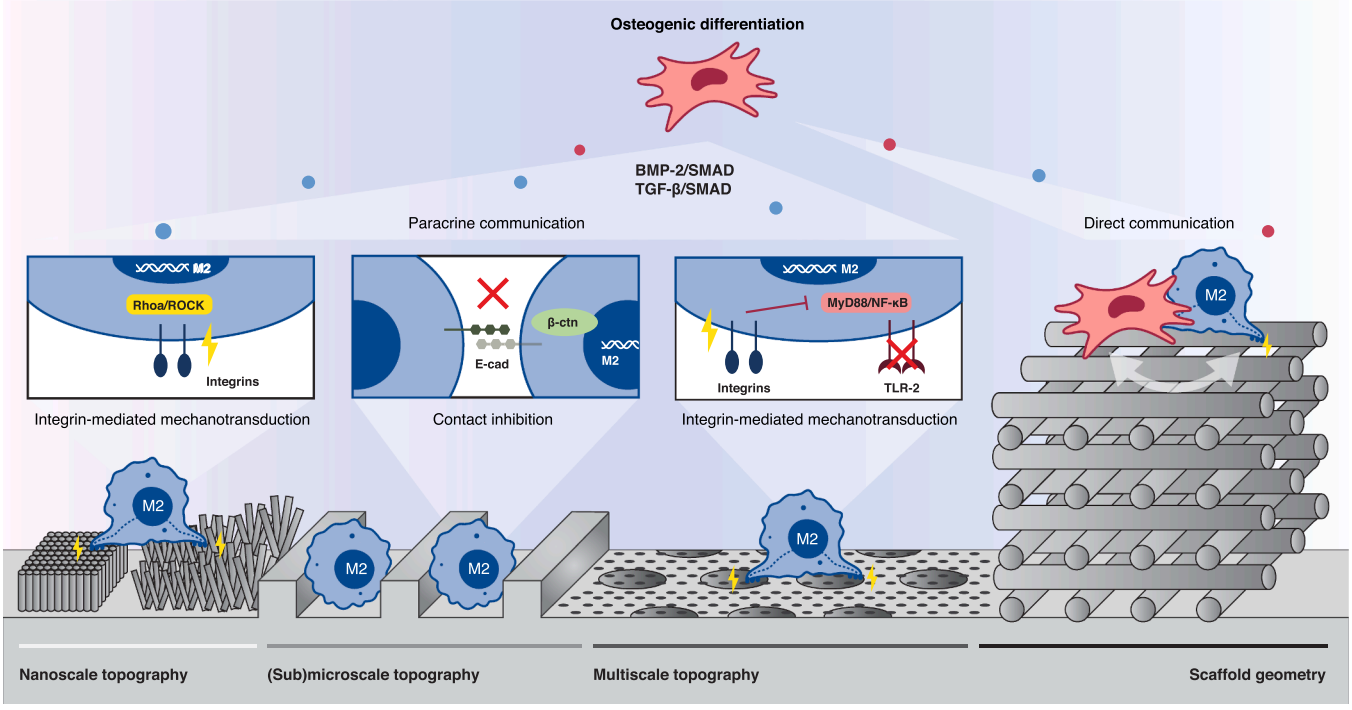

Fig. 7. Schematic illustration displaying OIM geometries identified at different length scales, their representative mechanisms of immunomodulation and the OIM signaling pathways.

bone ingrowth facilitation, vascularization, and mechanical strength, it seems that this pore size range can fulfill multiple biofunctionalities and, therefore, deserves more attention in future biomaterial designs [64]. Furthermore, grooved pores with high circularity show OIM properties. Importantly, this is not necessarily a fully circular pore, as hexagonal pores also possess a high circularity and provide more mechanical strength due to more load-bearing contact points [61].

Even though this review is focused on G-OIM, it is crucial to mention that changes in biomaterial geometry alter more than just shape: it can change the local chemical environment (*e.g.*, generation of chemical gradients due to confined geometries) and the surface chemistry (*e.g.*, protein adsorption profiles, apatite forming ability and ion release profiles), all of which influence cellular responses [65–67]. In multiple studies reviewed, the OIM geometries exhibited higher protein adsorption rates compared to those that did not induce successful OIM, demonstrating the importance of this phenomenon [44,38,42,47,50]. Therefore, geometry-induced chemical changes should be considered when evaluating the cellular responses.

3.2. G-OIM pathways

Various G-OIM mechanisms have been identified in this review. Primarily, a distinction can be made between pro-inflammatory and anti-inflammatory-mediated G-OIM. While initially only M2 macrophages were thought to be involved in bone regeneration, evidence shows that M1 macrophages also hold osteogenic potential [68–70]. In addition, based on the results found, there seems to be a correlation between the geometrical length scale and the ensuing course of G-OIM.

On nanoscale and multiscale topographies, M2-G-OIM is dominant and mainly achieved through BMP-2/SMAD and TGF-β/SMAD [44,42,50] (Fig. 7). Topography-induced mechanotransduction pathways (*e.g.,* RhoA/ROCK and PI3K/Akt1) enable M2 polarization of macrophages [44,39,42]. More varying mechanisms are involved at the microscale. M1-G-OIM occurs with geometries that target MAPK and NF-κB activation in macrophages, such as microrough substrates [34], hollow whiskers [47], and micropores produced by micro-arc oxidation (MAO) [35]. In addition to the already established osteogenic role of OSM produced by M1 macrophages [71], TNF-α has a concentration-dependent osteogenic effect, as lower concentrations lead to enhanced expression of Bmp2, Osx, Runx2 and osteocalcin in osteoprogenitors [47,72].

On scaffolds, M2-G-OIM is dominant. As the presence of BMP-2 and TGF-β was often not included in the secretome analysis, activation of BMP-2/SMAD and TGF-β/SMAD pathways by the OIM scaffolds was not confirmed. However, the decreased presence of IL-6 in the MCM was found beneficial for osteogenesis *via* the MAPK pathway in mMSCs in one study [60]. A notable and potent OIM mechanism is through direct cell-cell communication, which can induce high rates of osteogenesis regardless of geometry and without a dominant macrophage polarization state, as seen in a direct coculture model by Sridharan *et al.* [26] (Fig. 7).

It is unknown whether M1-, M1/M2- or M2-G-OIM is optimal. Referring to physiological events during inflammation, an M1-M2 shift may be the most relevant for OIM, as also revealed in a few studies in this review [39,42,51,55,29]. Biomaterial geometries should facilitate this polarization shift instead of strongly enhancing or prolonging an M1 or M2 state. For detecting and studying the effects of this polarization shift, transwell and direct coculture models are preferred over MCM, as the polarization shift is caused by bidirectional dynamic interactions, which MCM models do not capture. As seen in transwell studies, initial M1 polarization stimulates osteoprogenitor recruitment to the substrates seeded with the macrophages in the lower chamber [39,73]. Upon migration, a polarization shift to M2 can occur, presumably mediated by altered interactions between macrophages and migrated osteoprogenitors [39,73] (known to occur through prostaglandin-2 and cyclooxygenase-2 [44,68]). Furthermore, when both cell types are present on the substrate, the interplay between the substrate and the cells is essential for G-OIM and involves both paracrine and cell-cell communication [26,27].

Together, this indicates that an initial M1 response may benefit osteoprogenitor recruitment. In addition, an initial M1 response is indispensable after surgery to minimize the risk of infection and other surgery-related complications [70].

3.3. In vitro models

A clear limitation related to the current *in vitro* OIM models is the use of predominantly indirect and sometimes biologically irrelevant coculture models. Multiple studies in this review reported different rates of osteogenesis of the same geometry when translating from monoculture and MCM to more complex coculture or *in vivo* models. This indicates that monoculture and MCM models alone are insufficient for translational research. Indirect coculture models lack dynamic bidirectional communication and physical interactions that influence macrophage and osteoprogenitor behavior. The timing of medium refreshment and transfer is crucial, and determining the "optimum time point" is challenging. Discrepancies between studies make true comparative analysis difficult. Moreover, secreted factors in MCM may degrade or lose bioactivity over time, reducing their physiological relevance. Of note, to sustain the cocultured osteoprogenitor cell type, MCM is diluted with varying ratios of osteogenic medium, to find a medium composition that supports both cell types [74]. Furthermore, immunologically incompatible cell origins were sometimes used in coculture models [30,31–35]. Beside decreased scientific relevance, this may give skewed results and should be avoided altogether by using cells from compatible sources. Another limitation is the persisting use of osteogenic supplements (studies marked with * in Tables 1,3,5,6). Using culture media without osteogenic supplements helps establish biomaterial geometry's role for OIM.

Numerous improvements can be suggested regarding the representability of *in vitro* models for OIM. Regarding the nature of the coculture model, both transwell and direct coculture models should be used to capture the role of both paracrine signaling and direct cell-cell interactions. The transwell system can be used to assess the role of specific macrophage cytokines and chemokines in MSC migration, as well as the involvement of MSCs in orchestrating polarization switches, while the direct coculture model facilitates physiologically relevant cellular interactions. Choosing clinically relevant cell sources and polarization protocols is crucial for translational relevance. Many studies included in this review used the murine macrophage cell line RAW264.7, and only 2 studies used primary macrophages. Since murine macrophages differ substantially from human macrophages in *e.g.,* the NO and arginase metabolism [75], the cell origin is an important consideration in the study that achieved G-OIM by mediating the RAW264.7 NO metabolism using porous substrates [46]. Remarkably, of the 37 reviewed studies, only 1 study utilized human macrophages. In this study, the human monocyte-derived THP-1 cell line was used, which is the most frequently used human macrophage model. Treatment with 5-200 ng/mL phorbol 12-myristate 13-acetate for 24-72 hours is typically reported to induce macrophage differentiation, followed by stimulation with M1 (lipopolysaccharide + interferon-γ) and M2 (IL-4 + IL-13) stimuli [76]. However, there is currently no consensus on the starting state of macrophages upon seeding on the biomaterials and coculture. From a clinical perspective, initiating coculture with pre-stimulated M1 macrophages is more relevant for the *in vivo* post-operative inflammatory phase, allowing biomaterials to either initiate the polarization shift or prolong the inflammatory phase. However, the experimental conditions should always be tailed to the specific research questions of interest.

In terms of macrophage phenotypic validation, various researchers have correlated macrophage morphology with their polarization state [77,78]. This is controversial, as geometries can induce morphological

changes with and without affecting polarization [79,80]. Therefore, a robust, multi-modal approach is necessary, such as molecular analysis of standardized M1/M2 biomarkers at both the gene and protein levels, including surface and soluble biomarkers. However, where certain markers are consistently used for murine macrophages (*e.g.*, CD86, CD206, Arg1, iNOS for RAW264.7), this consistency is absent for human cell lines. Furthermore, it is important to remember that the M1/M2 classification of macrophages is an oversimplification that disregards M2 subtypes and transient states. Recent advances in single-cell RNA sequencing have revealed distinct subtypes, including M2a, M2b, and M2c, as well as transitional and hybrid phenotypes. Future studies should adopt multi-marker strategies or transcriptomic profiling to more accurately reflect macrophage heterogeneity and clarify the roles and presence of the different macrophage subtypes during OIM.

Notably, no coculture studies involving immune cells other than macrophages have been found to induce OIM, despite increasing discoveries regarding the role of B cells, T cells and neutrophils during bone metabolism [12]. This immediately reveals a significant knowledge gap. However, topography-induced B cell and T cell modulation has been investigated, forming a novel platform for achieving G-OIM through both the innate and the adaptive immune system. Wavy substrates can be used to instruct B and T cells [81,82]. Briefly, Myosin-II-inhibited T-cells remain in concave areas, whereas lamellipodia-inhibited T-cells cross ridges [81]. Furthermore, Ketchum *et al.* [82] developed nano-topographical surfaces to demonstrate that B cell activation can be modulated through topographical cues. To further predict the clinical performance of G-OIM biomaterials, *in vitro* models have already been expanded with human umbilical vein endothelial cells (HUVECs) to evaluate the biomaterial's potential for inducing angiogenesis [18,30,31,37,56]. Including vasculogenesis/angiogenesis in coculture models may provide more insights into the hypothesis that a polarization shift during the inflammatory and regenerative process is necessary, as M1 and M2 macrophages target different phases of angiogenesis *in vivo* [14,83].

To conclude, a minimum experimental framework for OIM should ideally include human monocyte-derived macrophages cocultured with hMSCs, evaluated in both direct and transwell coculture models. Extensive multi-marker phenotyping should be employed to confirm macrophage polarization. This, as well as the osteogenic outcomes, should be assessed at biologically relevant timepoints, tailored to the specific research questions. Translation to primary cells and the incorporation of endothelial or adaptive immune cells can bring the models closer to the *in vivo* scenario.

3.4. Future outlook

OIM is a recent development in the field of orthopedic biomaterials. Whereas initially the field was focused on achieving OIM through (bio) chemical modification of the substrates, increasingly advanced geometry-based approaches are being explored, including bioinspired and multiscale topographies. An interesting characteristic of trabecular bone that has not yet been considered regarding G-OIM is its surface curvature. As trabecular bone has an average mean curvature close to zero [84], minimal-curvature scaffolds (examples being triply periodic minimal surfaces) are interesting candidates for G-OIM. At the micro-scale, curvature shows multifaceted potential by similarity to curved ECM fibers [85]: directing cell migration (also referred to as curvotaxis) [23,85,86], influencing the collective cell organization of MC3T3-E1 [87], affecting macrophage shape and spreading [79], and promoting osteogenesis through the cytoskeletal remodeling of MSCs and MC3T3-E1 [86,88]. Furthermore, scaffolds based on controlled curvature can stimulate recruitment and osteogenic differentiation of skeletal stem cells and the formation of type H vessels *in vivo* (mice) [89].

Additionally, exploring OIM geometries for antibacterial properties (*e.g.,* nanopillars, nanowires, and nanospikes [90]) is of interest, as the immune system is involved in removing pathogens following implantation. One of the causes of bone implant failure is implant-associated infections (IAI), with devastating effects on patients. There are currently limited clinical solutions to prevent IAI. Furthermore, geometry in combination with biochemical functionalization can provide innovative designs, functioning as drug reservoirs or release systems for bioactive molecules or antibiotics (seen in this review on TNTs with BMP-2 [36] and ions [38,41], marked with ** in Table 1). However, it is essential to consider that any alteration in geometry is accompanied with chemical changes, which must be considered when evaluating cellular responses.

To conclude, OIM biomaterials represent a significant and highly clinically relevant advancement that is expected to contribute to the future of orthopedic implants. The key to success in OIM biomaterials is the availability of *in vitro* coculture models and associated methodologies to assess OIM. In addition to the emergence of direct coculture models, upscaling these models to bioreactors and organ-on-a-chip models allows for the study of sustained *in vitro* tissue growth under dynamic conditions, bringing these models closer to clinical settings. This will contribute to reduced use of animal models and enable the use of human-derived cells and tissues, providing fundamental insights under relevant pathophysiological conditions. Moreover, recent FDA guidelines now increasingly recognize human-derived *in vitro* platforms as valid preclinical models, a shift that will rapidly accelerate the development and approval of biomaterials [91]. In this context, development of key enabling technologies, such as high-resolution 3D (bio) printing, is essential to produce clinically relevant biomaterials and living constructs with precisely defined geometries across length scales. This would allow an early and integrated design optimization, considering both the processability and biocompatibility of orthopedic biomaterials. Furthermore, immunomodulation is not only relevant in bone biology, but has also been of tremendous interest in the treatment of autoimmune diseases, wound healing, cardiovascular disease, and inflammation-related disorders. Therefore, geometry-based immunomodulation can be relevant in adjacent areas that use biomaterials, such as regenerative skin graft engineering, cardiovascular implants, or immunosuppressive drug-eluting systems.

4. Conclusions

At all classified length scales, geometries with distinct OIM potential were identified. Various immunomodulatory pathways have been revealed. These pathways demonstrate that both M1 and M2 macrophages may contribute to osteogenesis. The mechanisms of immunomodulation are closely linked to the length scale of the substrate geometry. At nano-submicron scale, topographies can activate integrin-mediated mechanotransduction pathways for M1 and M2 polarization. OIM geometries in these size ranges include TNTs and various (ECM-mimicking) nanostructures, such as nanowires, nanodots, and honeycombs. Including a feature in this size range in addition to microfeatures (resulting in multiscale topographies), and including different areas of isotropy in micropatterns were also beneficial for G-OIM. For organized 3D scaffolds, high circularity pores with a diameter of ~500 μm display OIM across different biomaterials. Thus far, researchers have predominantly utilized indirect coculture models to achieve and understand G-OIM, through paracrine interactions mediated by the geometries. Direct coculture, which facilitates direct contact between macrophages, osteoprogenitors, and biomaterials, may enable an increase of the osteogenic potential by orchestrating physiologically relevant cellular interactions. As the field of OIM is rapidly advancing, the employment of human-derived cells in these coculture models, as well as upscaling these models to bioreactors and organ-on-chips, is indispensable. In addition, advancements in biofabrication should enable the development of more clinically relevant biomaterials with OIM geometries. These efforts could establish G-OIM as a promising regenerative immunoengineering strategy for orthopedic implants.

Data availability

No data was used for the research described in the article.

CRediT authorship contribution statement

Indra Mooij: Writing – review & editing, Writing – original draft, Visualization, Investigation, Conceptualization. **Iulian Apachitei:** Writing – review & editing, Supervision, Project administration, Funding acquisition, Conceptualization. **Amir A. Zadpoor:** Writing – review & editing, Supervision, Funding acquisition, Conceptualization. **Lidy E. Fratila-Apachitei:** Writing – review & editing, Visualization, Supervision, Investigation, Conceptualization.

Declaration of competing interest

The authors declare that they have no known competing financial interests or personal relationships that could have appeared to influence the work reported in this paper.

Acknowledgments

The research for this paper was financially supported by the PRosPERoS-II project, funded by the Interreg VA Flanders—the Netherlands program, CCI grant no. 2021TC16RFCB041.

References

[1] A.D. Woolf, B. Pfleger, Burden of major musculoskeletal conditions, Bull. World Health Organ. 81 (2003) 646–656.
[2] A.H. Schmidt, Autologous bone graft: is it still the gold standard? Injury 52 (2021) S18–S22, https://doi.org/10.1016/j.injury.2021.01.043.
[3] D. Xiao, J. Zhang, C. Zhang, D. Barbieri, H. Yuan, L. Moroni, G. Feng, The role of calcium phosphate surface structure in osteogenesis and the mechanisms involved, ACTA Biomater 106 (2020) 22–33, https://doi.org/10.1016/j.actbio.2019.12.034.
[4] C. Montoya, Y. Du, A.L. Gianforcaro, S. Orrego, M. Yang, P.I. Lelkes, On the road to smart biomaterials for bone research: definitions, concepts, advances, and outlook, Bone Res 9 (2021) 12, https://doi.org/10.1038/s41413-020-00131-z.
[5] N. Eliaz, N. Metoki, Calcium phosphate bioceramics: A review of their history, structure, properties, coating technologies and biomedical applications, Materials 10 (2017) 334, https://doi.org/10.3390/ma10040334.
[6] Z. Wang, M. Zhang, Z. Liu, Y. Wang, W. Dong, S. Zhao, D. Sun, Biomimetic design strategy of complex porous structure based on 3D printing Ti-6Al-4V scaffolds for enhanced osseointegration, Mater. Des. 218 (2022) 110721, https://doi.org/10.1016/j.matdes.2022.110721.
[7] Y. Zheng, Q. Han, J. Wang, D. Li, Z. Song, J. Yu, Promotion of osseointegration between implant and bone interface by titanium alloy porous scaffolds prepared by 3D printing, ACS Biomater. Sci. Eng. 6 (2020) 5181–5190, https://doi.org/10.1021/acsbiomaterials.0c00662.
[8] R. Alkentar, N. Kladovasilakis, D. Tzetzis, T. Mankovits, Effects of pore size parameters of titanium additively manufactured lattice structures on the osseointegration process in orthopedic applications: A comprehensive review, Crystals 13 (2023) 113, https://doi.org/10.3390/cryst13010113.
[9] Z. Chen, T. Klein, R.Z. Murray, R. Crawford, J. Chang, C. Wu, Y. Xiao, Osteoimmunomodulation for the development of advanced bone biomaterials, Mater. Today 19 (2016) 304–321, https://doi.org/10.1016/j.mattod.2015.11.004.
[10] Y. Xie, C. Hu, Y. Feng, D. Li, T. Ai, Y. Huang, X. Chen, L. Huang, J. Tan, Osteoimmunomodulatory effects of biomaterial modification strategies on macrophage polarization and bone regeneration, Regen. Biomater. 7 (2020) 233–245, https://doi.org/10.1093/rb/rbaa006.
[11] C. Guder, S. Gravius, C. Burger, D.C. Wirtz, F.A. Schildberg, Osteoimmunology: A current update of the interplay between bone and the immune system, Front. Immunol. 11 (2020) 58, https://doi.org/10.3389/fimmu.2020.00058.
[12] R.J. Miron, M. Bohner, Y. Zhang, D.D. Bosshardt, Osteoinduction and osteoimmunology: emerging concepts, Periodontol 2000 (2023) prd.12519, https://doi.org/10.1111/prd.12519.
[13] H. Takayanagi, K. Ogasawara, S. Hida, T. Chiba, S. Murata, K. Sato, A. Takaoka, T. Yokochi, H. Oda, K. Tanaka, K. Nakamura, T. Taniguchi, T-cell-mediated regulation of osteoclastogenesis by signalling cross-talk between RANKL and IFN-γ, Nature 408 (2000) 600–605, https://doi.org/10.1038/35046102.
[14] Z. Song, Y. Cheng, M. Chen, X. Xie, Macrophage polarization in bone implant repair: A review, Tissue Cell 82 (2023) 102112, https://doi.org/10.1016/j.tice.2023.102112.
[15] A. Curtis, C. Wilkinson, Topographical control of cells, Biomaterials 18 (1997) 1573–1583, https://doi.org/10.1016/S0142-9612(97)00144-0.
[16] B. Wójciak-Stothard, A. Curtis, W. Monaghan, K. Macdonald, C. Wilkinson, Guidance and activation of murine macrophages by nanometric scale topography, Exp. Cell Res. 223 (1996) 426–435, https://doi.org/10.1006/excr.1996.0098.
[17] Z. Chen, A. Bachhuka, S. Han, F. Wei, S. Lu, R.M. Visalakshan, K. Vasilev, Y. Xiao, Tuning chemistry and topography of nanoengineered surfaces to manipulate immune response for bone regeneration applications, ACS Nano 11 (2017) 4494–4506, https://doi.org/10.1021/acsnano.6b07808.
[18] J. Wang, S. Qian, X. Liu, L. Xu, X. Miao, Z. Xu, L. Cao, H. Wang, X. Jiang, M2 macrophages contribute to osteogenesis and angiogenesis on nanotubular TiO2 surfaces, J. Mater. Chem. B 5 (2017) 3364–3376, https://doi.org/10.1039/C6TB03364D.
[19] Y. He, M. Tian, X. Li, J. Hou, S. Chen, G. Yang, X. Liu, S. Zhou, A hierarchical-structured mineralized nanofiber scaffold with osteoimmunomodulatory and osteoinductive functions for enhanced alveolar bone regeneration, Adv. Healthc. Mater. 11 (2022) 2102236, https://doi.org/10.1002/adhm.202102236.
[20] Y. Alex, S. Vincent, N. Divakaran, U.T. Uthappa, P. Srinivasan, S. Mubarak, M. A. Al-Harthi, D. Dhamodharan, Pioneering bone regeneration: A review of cutting-edge scaffolds in tissue engineering, Bioprinting 43 (2024) e00364, https://doi.org/10.1016/j.bprint.2024.e00364.
[21] A. Barlian, K. Vanya, Nanotopography in directing osteogenic differentiation of mesenchymal stem cells: potency and future perspective, Future Sci. OA 8 (2022) FSO765, https://doi.org/10.2144/fsoa-2021-0097.
[22] A.W. James, G. LaChaud, J. Shen, G. Asatrian, V. Nguyen, X. Zhang, K. Ting, C. Soo, A review of the clinical side effects of bone morphogenetic protein-2, Tissue Eng. Part B Rev. 22 (2016) 284–297, https://doi.org/10.1089/ten.teb.2015.0357.
[23] L. Pieuchot, J. Marteau, A. Guignandon, T. Dos Santos, I. Brigaud, P.-F. Chauvy, T. Cloatre, A. Ponche, T. Petithory, P. Rougerie, M. Vassaux, J.-L. Milan, N. Tusamda Wakhloo, A. Spangenberg, M. Bigerelle, K. Anselme, Curvotaxis directs cell migration through cell-scale curvature landscapes, Nat. Commun. 9 (2018) 3995, https://doi.org/10.1038/s41467-018-06494-6.
[24] Y. Zhang, T. Böse, R.E. Unger, J.A. Jansen, C.J. Kirkpatrick, J.J.J.P. van den Beucken, Macrophage type modulates osteogenic differentiation of adipose tissue MSCs, Cell Tissue Res 369 (2017) 273–286, https://doi.org/10.1007/s00441-017-2598-8.
[25] F. Loi, L.A. Córdova, R. Zhang, J. Pajarinen, T. Lin, S.B. Goodman, Z. Yao, The effects of immunomodulation by macrophage subsets on osteogenesis in vitro, Stem Cell Res. Ther. 7 (2016) 15, https://doi.org/10.1186/s13287-016-0276-5.
[26] R. Sridharan, K.J. Genoud, D.J. Kelly, F.J. O'Brien, Hydroxyapatite particle shape and size influence MSC osteogenesis by directing the macrophage phenotype in collagen-Hydroxyapatite scaffolds, ACS Appl. Bio Mater 3 (2020) 7562–7574, https://doi.org/10.1021/acsabm.0c00801.
[27] M. Nouri-Goushki, B.I.M. Eijkel, M. Minneboo, L.E. Fratila-Apachitei, A. A. Zadpoor, Osteoimmunomodulatory potential of 3D printed submicron patterns assessed in a direct co-culture model, Biomater. Adv. 139 (2022) 212993, https://doi.org/10.1016/j.bioadv.2022.212993.
[28] J. Wang, F. Meng, W. Song, J. Jin, Q. Ma, D. Fei, L. Fang, L. Chen, Q. Wang, Y. Zhang, Nanostructured titanium regulates osseointegration via influencing macrophage polarization in the osteogenic environment, Int. J. Nanomedicine 13 (2018) 4029–4043, https://doi.org/10.2147/IJN.S163956.
[29] H. Moon, K. Gulati, T. Li, C.S. Moran, S. Ivanovski, Inflammatory or reparative? Tuning macrophage polarization using anodized anisotropic nanoporous titanium implant surfaces, Small Sci (2024) 2400211, https://doi.org/10.1002/smsc.202400211.
[30] C. Yang, C. Zhao, X. Wang, M. Shi, Y. Zhu, L. Jing, C. Wu, J. Chang, Stimulation of osteogenesis and angiogenesis by micro/nano hierarchical hydroxyapatite via macrophage immunomodulation, Nanoscale 11 (2019) 17699–17708, https://doi.org/10.1039/C9NR05730G.
[31] S. Ni, D. Zhai, Z. Huan, T. Zhang, J. Chang, C. Wu, Nanosized concave pit/convex dot microarray for immunomodulatory osteogenesis and angiogenesis, Nanoscale 12 (2020) 16474–16488, https://doi.org/10.1039/D0NR03886E.
[32] W. Liu, L. Liang, B. Liu, D. Zhao, Y. Tian, Q. Huang, H. Wu, The response of macrophages and their osteogenic potential modulated by micro/nano-structured Ti surfaces, Colloids Surf. B Biointerfaces 205 (2021) 111848, https://doi.org/10.1016/j.colsurfb.2021.111848.
[33] J.M. Sadowska, F. Wei, J. Guo, J. Guillem-Marti, M.-P. Ginebra, Y. Xiao, Effect of nano-structural properties of biomimetic hydroxyapatite on osteoimmunomodulation, Biomaterials 181 (2018) 318–332, https://doi.org/10.1016/j.biomaterials.2018.07.058.
[34] X. Li, Q. Huang, T.A. Elkhooly, Y. Liu, H. Wu, Q. Feng, L. Liu, Y. Fang, W. Zhu, T. Hu, Effects of titanium surface roughness on the mediation of osteogenesis via modulating the immune response of macrophages, Biomed. Mater. 13 (2018) 045013, https://doi.org/10.1088/1748-605X/aabe33.
[35] X. Li, Q. Huang, X. Hu, D. Wu, N. Li, Y. Liu, Q. Li, H. Wu, Evaluating the osteoimmunomodulatory properties of micro-arc oxidized titanium surface at two different biological stages using an optimized in vitro cell culture strategy, Mater. Sci. Eng. C 110 (2020) 110722, https://doi.org/10.1016/j.msec.2020.110722.
[36] M. Ali, Y. He, A.S.N. Chang, A. Wu, J. Liu, Y. Cao, Y. Mohammad, A. Popat, L. Walsh, Q. Ye, C. Xu, T. Kumeria, Osteoimmune-modulating and BMP-2-eluting anodised 3D printed titanium for accelerated bone regeneration, J. Mater. Chem. B 12 (2023) 97–111, https://doi.org/10.1039/D3TB01029E.
[37] B. Tao, H. Lan, X. Zhou, C. Lin, X. Qin, M. Wu, Y. Zhang, S. Chen, A. Guo, K. Li, L. Chen, Y. Jiao, W. Yi, Regulation of TiO2 nanotubes on titanium implants to orchestrate osteo/angio-genesis and osteo-immunomodulation for boosted osseointegration, Mater. Des. 233 (2023) 112268, https://doi.org/10.1016/j.matdes.2023.112268.

[38] B. Chen, Y. You, A. Ma, Y. Song, J. Jiao, L. Song, E. Shi, X. Zhong, Y. Li, C. Li, Zn-incorporated TiO2 nanotube surface improves osteogenesis ability through influencing immunomodulatory function of macrophages, Int. J. Nanomedicine 15 (2020) 2095–2118, https://doi.org/10.2147/IJN.S244349.
[39] X. Shen, Y. Yu, P. Ma, Z. Luo, Y. Hu, M. Li, Y. He, Y. Zhang, Z. Peng, G. Song, K. Cai, Titania nanotubes promote osteogenesis via mediating crosstalk between macrophages and MSCs under oxidative stress, Colloids Surf. B Biointerfaces 180 (2019) 39–48, https://doi.org/10.1016/j.colsurfb.2019.04.033.
[40] X. Cao, R. Lu, X. Wang, C. Wang, Y. Zhao, Y. Sun, S. Chen, Hydrogenated TiO_2 nanotubes regulate osseointegration by influencing macrophage polarization in the osteogenic environment, J. Nanomater. 2022 (2022) e2650421, https://doi.org/10.1155/2022/2650421.
[41] X. Qiao, J. Yang, Y. Shang, S. Deng, S. Yao, Z. Wang, Y. Guo, C. Peng, Magnesium-doped nanostructured titanium surface modulates macrophage-mediated inflammatory response for ameliorative osseointegration, Int. J. Nanomedicine 15 (2020) 7185–7198, https://doi.org/10.2147/IJN.S239550.
[42] M. Yu, H. Yang, B. Li, R. Wang, Y. Han, Molecular mechanisms of interrod spacing-mediated osseointegration via modulating inflammatory response and osteogenic differentiation, Chem. Eng. J. 454 (2023) 140141, https://doi.org/10.1016/j.cej.2022.140141.
[43] N. Leijnse, Y.F. Barooji, M.R. Arastoo, S.L. Sønder, B. Verhagen, L. Wullkopf, J. T. Erler, S. Semsey, J. Nylandsted, L.B. Oddershede, A. Doostmohammadi, P. M. Bendix, Filopodia rotate and coil by actively generating twist in their actin shaft, Nat. Commun. 13 (2022) 1636, https://doi.org/10.1038/s41467-022-28961-x.
[44] K. Li, S. Liu, T. Hu, I. Razanau, X. Wu, H. Ao, L. Huang, Y. Xie, X. Zheng, Optimized nanointerface engineering of micro/nanostructured titanium implants to enhance cell–Nanotopography interactions and osseointegration, ACS Biomater. Sci. Eng. 6 (2020) 969–983, https://doi.org/10.1021/acsbiomaterials.9b01717.
[45] Z. Chen, S. Ni, S. Han, R. Crawford, S. Lu, F. Wei, J. Chang, C. Wu, Y. Xiao, Nanoporous microstructures mediate osteogenesis by modulating the osteo-immune response of macrophages, Nanoscale 9 (2017) 706–718, https://doi.org/10.1039/C6NR06421C.
[46] X. Liu, L. Ouyang, L. Chen, Y. Qiao, X. Ma, G. Xu, X. Liu, Hydroxyapatite composited PEEK with 3D porous surface enhances osteoblast differentiation through mediating NO by macrophage, Regen. Biomater. 9 (2022) rbab076, https://doi.org/10.1093/rb/rbab076.
[47] J. Wang, H. Li, S. Fu, Y. Su, Porous BCP ceramics with nanoscale whisker structure accelerate bone regeneration by regulating inflammatory response, Biomater. Adv. 147 (2023) 213313, https://doi.org/10.1016/j.bioadv.2023.213313.
[48] Z. Zhang, Y. Xie, H. Pan, L. Huang, X. Zheng, Influence of patterned titanium coatings on polarization of macrophage and osteogenic differentiation of bone marrow stem cells, J. Biomater. Appl. 32 (2018) 977–986, https://doi.org/10.1177/0885328217746802.
[49] Y. Zhu, H. Liang, X. Liu, J. Wu, C. Yang, T.M. Wong, K.Y.H. Kwan, K.M.C. Cheung, S. Wu, K.W.K. Yeung, Regulation of macrophage polarization through surface topography design to facilitate implant-to-bone osteointegration, Sci. Adv. 7 (2021) eabf6654, https://doi.org/10.1126/sciadv.abf6654.
[50] J. Wu, C. Feng, M. Wang, H. Wu, X. Zhu, X. Li, X. Chen, X. Zhang, Whisker of biphasic calcium phosphate ceramics: osteo-immunomodulatory behaviors, Nano Res 15 (2022) 9169–9182, https://doi.org/10.1007/s12274-022-4591-0.
[51] J. Wang, Y. Su, L. Xu, D. Li, Micro-patterned surface construction on BCP ceramics and the regulation on inflammation-involved osteogenic differentiation, Mater. Sci. Eng. C 116 (2020) 111220, https://doi.org/10.1016/j.msec.2020.111220.
[52] S. Chen, A.F.U.H. Saeed, Q. Liu, Q. Jiang, H. Xu, G.G. Xiao, L. Rao, Y. Duo, Macrophages in immunoregulation and therapeutics, Signal Transduct. Target. Ther 8 (2023) 1–35, https://doi.org/10.1038/s41392-023-01452-1.
[53] B.A. Otálora-Otálora, B. Henríquez, L. López-Kleine, A. Rojas, RUNX family: oncogenes or tumor suppressors (Review), Oncol. Rep. 42 (2019) 3–19, https://doi.org/10.3892/or.2019.7149.
[54] Y. Yang, T. Zhang, M. Jiang, X. Yin, X. Luo, H. Sun, Effect of the immune responses induced by implants in a integrated three-dimensional micro-nano topography on osseointegration, J. Biomed. Mater. Res. A 109 (2021) 1429–1440, https://doi.org/10.1002/jbm.a.37134.
[55] X. Dai, Y. Bai, B.C. Heng, Y. Li, Z. Tang, C. Lin, O. Liu, Y. He, X. Zhang, X. Deng, Biomimetic hierarchical implant surfaces promote early osseointegration in osteoporotic rats by suppressing macrophage activation and osteoclastogenesis, J. Mater. Chem. B 10 (2022) 1875–1885, https://doi.org/10.1039/D1TB02871E.
[56] H. Pan, Y. Xie, Z. Zhang, K. Li, D. Hu, X. Zheng, T. Tang, Immunomodulation effect of a hierarchical macropore/nanosurface on osteogenesis and angiogenesis, Biomed. Mater. 12 (2017) 045006, https://doi.org/10.1088/1748-605X/aa6b7c.
[57] X. Zheng, L. Chen, J. Tan, J. Miao, X. Liu, T. Yang, Z. Ding, Effect of micro/nano-sheet array structures on the osteo-immunomodulation of macrophages, Regen. Biomater. 9 (2022) rbac075, https://doi.org/10.1093/rb/rbac075.
[58] Y. Xuan, L. Li, C. Zhang, M. Zhang, J. Cao, Z. Zhang, The 3D-printed ordered bredigite scaffold promotes pro-healing of critical-sized bone defects by regulating macrophage polarization, Int. J. Nanomedicine 18 (2023) 917–932, https://doi.org/10.2147/IJN.S393080.
[59] X. Wang, X. Fu, D. Luo, R. Hou, P. Li, Y. Chen, X. Zhang, X. Meng, Y. Yue, J. Liu, 3D printed high-precision porous scaffolds prepared by fused deposition modeling induce macrophage polarization to promote bone regeneration, Biomed. Mater. 19 (2024) 035006, https://doi.org/10.1088/1748-605X/ad2ed0.
[60] C. Li, L. Yang, X. Ren, M. Lin, X. Jiang, D. Shen, T. Xu, J. Ren, L. Huang, W. Qing, J. Zheng, Y. Mu, Groove structure of porous hydroxyapatite scaffolds (HAS) modulates immune environment via regulating macrophages and subsequently enhances osteogenesis, JBIC J. Biol. Inorg. Chem. 24 (2019) 733–745, https://doi.org/10.1007/s00775-019-01687-w.
[61] Y. Wu, Z. Liu, Z. Xu, Y. Zhang, H. Ye, X. Wang, Macrophage responses to selective laser-melted Ti-6Al-4V scaffolds of different pore geometries and the corresponding osteoimmunomodulatory effects toward osteogenesis, J. Biomed. Mater. Res. A 110 (2022) 873–883, https://doi.org/10.1002/jbm.a.37335.
[62] X. Yu, Y. Wang, M. Zhang, H. Ma, C. Feng, B. Zhang, X. Wang, B. Ma, Q. Yao, C. Wu, 3D printing of gear-inspired biomaterials: immunomodulation and bone regeneration, Acta Biomater 156 (2023) 222–233, https://doi.org/10.1016/j.actbio.2022.09.008.
[63] Y. Guo, L. Li, J. Gao, X. Chen, Q. Sang, miR-214 suppresses the osteogenic differentiation of bone marrow-derived mesenchymal stem cells and these effects are mediated through the inhibition of the JNK and p38 pathways, Int. J. Mol. Med. 39 (2017) 71–80, https://doi.org/10.3892/ijmm.2016.2826.
[64] X.P. Tan, Y.J. Tan, C.S.L. Chow, S.B. Tor, W.Y. Yeong, Metallic powder-bed based 3D printing of cellular scaffolds for orthopaedic implants: A state-of-the-art review on manufacturing, topological design, mechanical properties and biocompatibility, Mater. Sci. Eng. C 76 (2017) 1328–1343, https://doi.org/10.1016/j.msec.2017.02.094.
[65] M. Bohner, R.J. Miron, A proposed mechanism for material-induced heterotopic ossification, Mater. Today 22 (2019) 132–141, https://doi.org/10.1016/j.mattod.2018.10.036.
[66] S. Fujibayashi, M. Neo, H.-M. Kim, T. Kokubo, T. Nakamura, Osteoinduction of porous bioactive titanium metal, Biomaterials 25 (2004) 443–450, https://doi.org/10.1016/S0142-9612(03)00551-9.
[67] J. Chen, J. Dai, J. Qian, W. Li, R. Li, D. Pang, G. Wan, P. Li, S. Xu, Influence of surface roughness on biodegradability and cytocompatibility of high-purity magnesium, Materials (Basel) 15 (2022) 3991, https://doi.org/10.3390/ma15113991.
[68] L.Y. Lu, F. Loi, K. Nathan, T.-H. Lin, J. Pajarinen, E. Gibon, A. Nabeshima, L. Cordova, E. Jämsen, Z. Yao, S.B. Goodman, Pro-inflammatory M1 macrophages promote osteogenesis by mesenchymal stem cells via the COX-2-prostaglandin E2 pathway, J. Orthop. Res. Off. Publ. Orthop. Res. Soc. 35 (2017) 2378–2385, https://doi.org/10.1002/jor.23553.
[69] J. Yang, G. Chen, T. Fan, X. Qu, M1 macrophage-derived oncostatin M induces osteogenic differentiation of ligamentum flavum cells through the JAK2/STAT3 pathway, JOR SPINE 7 (2024) e1290, https://doi.org/10.1002/jsp2.1290.
[70] D. Zhang, Y. Dang, R. Deng, Y. Ma, J. Wang, J. Ao, X. Wang, Research progress of macrophages in bone regeneration, J. Tissue Eng. Regen. Med. 2023 (2023) 1512966, https://doi.org/10.1155/2023/1512966.
[71] P. Guihard, Y. Danger, B. Brounais, E. David, R. Brion, J. Delecrin, C.D. Richards, S. Chevalier, F. Rédini, D. Heymann, H. Gascan, F. Blanchard, Induction of osteogenesis in mesenchymal stem cells by activated monocytes/macrophages depends on oncostatin M signaling, Stem Cells 30 (2012) 762–772, https://doi.org/10.1002/stem.1040.
[72] B. Osta, G. Benedetti, P. Miossec, Classical and paradoxical effects of TNF-α on bone homeostasis, Front. Immunol. 5 (2014) 48, https://doi.org/10.3389/fimmu.2014.00048.
[73] D. Yu, S. Guo, D. Yang, B. Li, Z. Guo, Y. Han, Interrod spacing dependent angiogenesis and osseointegration of Na2TiO3 nanorods-patterned arrays *via* immunoregulation, Chem. Eng. J. 426 (2021) 131187, https://doi.org/10.1016/j.cej.2021.131187.
[74] G. Mestres, S.-S.D. Carter, N.P. Hailer, A. Diez-Escudero, A practical guide for evaluating the osteoimmunomodulatory properties of biomaterials, Acta Biomater 130 (2021) 115–137, https://doi.org/10.1016/j.actbio.2021.05.038.
[75] F.O. Martinez, L. Helming, S. Gordon, Alternative activation of macrophages: an immunologic functional perspective, Annu. Rev. Immunol. 27 (2009) 451–483, https://doi.org/10.1146/annurev.immunol.021908.132532.
[76] P. Phuangbubpha, S. Thara, P. Sriboonaied, P. Saetan, W. Tumnoi, A. Charoenpanich, Optimizing THP-1 macrophage culture for an immune-responsive Human intestinal model, Cells 12 (2023) 1427, https://doi.org/10.3390/cells12101427.
[77] F.Y. McWhorter, T. Wang, P. Nguyen, T. Chung, W.F. Liu, Modulation of macrophage phenotype by cell shape, Proc. Natl. Acad. Sci. 110 (2013) 17253–17258, https://doi.org/10.1073/pnas.1308887110.
[78] M. Selig, L. Poehlman, N.C. Lang, M. Völker, B. Rolauffs, M.L. Hart, Prediction of six macrophage phenotypes and their IL-10 content based on single-cell morphology using artificial intelligence, Front. Immunol. 14 (2024), https://doi.org/10.3389/fimmu.2023.1336393.
[79] V. Malheiro, F. Lehner, V. Dinca, P. Hoffmann, K. Maniura-Weber, Convex and concave micro-structured silicone controls the shape, but not the polarization state of human macrophages, Biomater. Sci. 4 (2016) 1562–1573, https://doi.org/10.1039/C6BM00425C.
[80] N. Jain, V. Vogel, Spatial confinement downsizes the inflammatory response of macrophages, Nat. Mater. 17 (2018) 1134–1144, https://doi.org/10.1038/s41563-018-0190-6.
[81] K.H. Song, S.J. Park, D.S. Kim, J. Doh, Sinusoidal wavy surfaces for curvature-guided migration of T lymphocytes, Biomaterials 51 (2015) 151–160, https://doi.org/10.1016/j.biomaterials.2015.01.071.
[82] C.M. Ketchum, X. Sun, A. Suberi, J.T. Fourkas, W. Song, A. Upadhyaya, Subcellular topography modulates actin dynamics and signaling in B-cells, Mol. Biol. Cell 29 (2018) 1732–1742, https://doi.org/10.1091/mbc.E17-06-0422.
[83] P.L. Graney, S. Ben-Shaul, S. Landau, A. Bajpai, B. Singh, J. Eager, A. Cohen, S. Levenberg, K.L. Spiller, Macrophages of diverse phenotypes drive vascularization of engineered tissues, Sci. Adv 6 (2020) eaay6391, https://doi.org/10.1126/sciadv.aay6391.

[84] C.M. Bidan, F.M. Wang, J.W.C. Dunlop, A three-dimensional model for tissue deposition on complex surfaces, Comput. Methods Biomech. Biomed. Engin. 16 (2013) 1056–1070, https://doi.org/10.1080/10255842.2013.774384.
[85] M. Luciano, C. Tomba, A. Roux, S. Gabriele, How multiscale curvature couples forces to cellular functions, Nat. Rev. Phys. 6 (2024) 246–268, https://doi.org/10.1038/s42254-024-00700-9.
[86] M. Werner, S.B.G. Blanquer, S.P. Haimi, G. Korus, J.W.C. Dunlop, G.N. Duda, Dirk. W. Grijpma, A. Petersen, Surface curvature differentially regulates stem cell migration and differentiation via altered attachment morphology and nuclear deformation, Adv. Sci. 4 (2017) 1600347, https://doi.org/10.1002/advs.201600347.
[87] S.J.P. Callens, D. Fan, I.A.J. Van Hengel, M. Minneboo, P.J. Díaz-Payno, M. M. Stevens, L.E. Fratila-Apachitei, A.A. Zadpoor, Emergent collective organization of bone cells in complex curvature fields, Nat. Commun. 14 (2023) 855, https://doi.org/10.1038/s41467-023-36436-w.
[88] H. Wu, Y. Liu, C. Ai, S. Shi, R.H.W. Lam, J. Hu, Cell-scale microstructures promote osteogenic differentiation of MC3T3-E1 cells, Colloids Surf. Physicochem. Eng. Asp. 676 (2023) 132197, https://doi.org/10.1016/j.colsurfa.2023.132197.
[89] Y. Liu, Y. Wang, M. Lin, H. Liu, Y. Pan, J. Wu, Z. Guo, J. Li, B. Yan, H. Zhou, Y. Fan, G. Hu, H. Liang, S. Zhang, M.F. Siu, Y. Wu, J. Bai, C. Liu, Cellular scale curvature in bioceramic scaffolds enhanced bone regeneration by regulating skeletal stem cells and vascularization, Adv. Healthc. Mater. (2024) 2401667, https://doi.org/10.1002/adhm.202401667.
[90] K. Modaresifar, S. Azizian, M. Ganjian, L.E. Fratila-Apachitei, A.A. Zadpoor, Bactericidal effects of nanopatterns: A systematic review, Acta Biomater 83 (2019) 29–36, https://doi.org/10.1016/j.actbio.2018.09.059.
[91] U.S. Food and Drug Administration, FDA Announces Plan to Phase Out Animal Testing Requirement for Monoclonal Antibodies and Other Drugs, FDA, 2025. https://www.fda.gov/news-events/press-announcements/fda-announces-plan-phase-out-animal-testing-requirement-monoclonal-antibodies-and-other-drugs. accessed June 6, 2025.